



HAL
open science

Cooperative Anion- π and C–H–Cl Interactions in Multifunctional Naphthalene-Based Receptors for Chloride Recognition: Cage-Size Modulation Through Substitution Patterns

Olfa Zayene, Jun Hu, Aurélie Damond, Chantal Roc, Jérôme Marrot, Anne Gaucher, Jean-Yves Salpin, Damien Prim

► To cite this version:

Olfa Zayene, Jun Hu, Aurélie Damond, Chantal Roc, Jérôme Marrot, et al.. Cooperative Anion- π and C–H–Cl Interactions in Multifunctional Naphthalene-Based Receptors for Chloride Recognition: Cage-Size Modulation Through Substitution Patterns. ChemPlusChem, 2024, pp.e202400380. 10.1002/cplu.202400380 . hal-04750470

HAL Id: hal-04750470

<https://hal.science/hal-04750470v1>

Submitted on 23 Oct 2024

HAL is a multi-disciplinary open access archive for the deposit and dissemination of scientific research documents, whether they are published or not. The documents may come from teaching and research institutions in France or abroad, or from public or private research centers.

L'archive ouverte pluridisciplinaire **HAL**, est destinée au dépôt et à la diffusion de documents scientifiques de niveau recherche, publiés ou non, émanant des établissements d'enseignement et de recherche français ou étrangers, des laboratoires publics ou privés.



Distributed under a Creative Commons Attribution - NonCommercial - NoDerivatives 4.0 International License

Cooperative Anion- π and C-H-Cl Interactions in Multifunctional Naphthalene-Based Receptors for Chloride Recognition: Cage-size Modulation Through Substitution Patterns

Olfa Zayene,^a Jun Hu,^{a,b} Aurélie Damond,^a Chantal Roc,^b Jérôme Marrot,^a Anne Gaucher,^{*,a} Jean-Yves Salpin,^b and Damien Prim,^{*,a}

^a *Université Paris-Saclay, UVSQ, CNRS, Institut Lavoisier de Versailles, 78035 Versailles cedex, France*

^b *Université Paris-Saclay, Univ Evry, CY Cergy Paris Université, CNRS, LAMBE, 91025, Evry-Courcouronnes, France*

Abstract

This study introduces a novel approach for chloride recognition utilizing multifunctional naphthalene-based receptors. By strategically modifying the substitution patterns on tetrafluoropyridines, a series of new receptors with customized cavities and enhanced binding capabilities were developed. Density functional theory (DFT) calculations and experimental studies combining NMR spectroscopy and mass spectrometry confirmed the efficacy of these receptors in capturing chloride ions. The relative chloride affinity order determined experimentally is in agreement with DFT predictions. The synergistic effect of anion- π and C-H...Cl interactions, mediated by the TFP groups, played a crucial role in achieving high binding affinity. This work provides valuable insights for designing future anion receptors with improved performance.

Introduction:

Anion recognition plays a crucial role in different fields, such as biology, environmental science, and catalysis, highlighting its significance and high relevance^[1,2]. As the range of applications extends^[3], research has intensified during the last decades, studying anion recognition both in solution and in the gas phase^[4-6]. One of the most investigated aspects in this field is the selectivity of receptors towards specific anions. In this context, the intrinsic properties of the anion, its basicity, geometry, size, and the architectural design of the receptor, which involves its flexibility or rigidity and the nature of the interactions involved, are essential parameters.

Among anions, chloride is ubiquitous in nature and plays a vital role in numerous biological processes^[1,3], environmental systems, chemical and industrial applications, making its precise recognition crucial. However, achieving its selectivity still needs to be improved^[7]. Discriminating between chloride and other anions, especially those of similar size and charge, remains an issue. Furthermore, the environmental prevalence of chloride demands receptors that are selective and highly sensitive under a broad range of conditions. This requires a comprehensive understanding of interaction mechanisms when designing receptor molecules to ensure chloride specificity.

This paper focuses on developing selective receptors for chloride. We have synthesized a series of receptors based on a rigid naphthalene spacer, decorated with tetrafluoropyridines (TFP) in various substitution patterns. Their 3D molecular architectures are tunable, the size of the cavities in which the chloride ion penetrates is modifiable, and the nature of the weak interactions and their cooperativity are modulable to yield receptors with variable cavity sizes.

Due to their π -acidic nature, TFP^[8] interact with the anion *via* anion- π interactions^[8-10]. Though less investigated in solution due to their relative weakness influenced by solvation, such interactions become pertinent to study in the gas phase^[5]. The topology of the receptors is confirmed *via* X-ray crystallography, while their complexation efficiency and selectivity are evaluated through Density Functional Theory (DFT) calculations and mass spectrometry.

Theoretical study

In this study, DFT helped predicting the geometry of the desired receptors and providing some insights in their chloride binding ability.

First, the receptors were optimized at the APFD/aug-cc-pvDZ level of theory^[4] with the Gaussian 16 set of programs. Each structure's local minimum was confirmed by ensuring the absence of imaginary frequencies. NCIPLOT analysis were performed (Figure 1). Symmetrical substitution patterns (2,7 and 1,8) as shown in compounds **1** and **3**, respectively, were first examined. The topology of receptor **1** is set by stabilizing interactions between fluorine atoms of the TFP moiety and the H1-C1-C2 fragment of the naphthalene ring. Also noteworthy are the relative positions of both TFP lying almost face-to-face with each other and almost perpendicular to the naphthalene plane. Similarly, the geometry of compound **3**, is defined by the relative orientations of the TFPs, which face each other. However, the spatial proximity of both heterocycles leads to an additional π - π stacking interaction, further stabilizing the receptor by c.a 12 kJ/mol (see supporting information for computed energies). In contrast to **1** and **3**, compound **2** exhibits a non-symmetrical substitution pattern (2,8), which induces a different tridimensional geometry. Interestingly, TFP located at position 2 adopts an overall similar conformation and thus exhibits similar stabilizing interactions compared to the one observed in compound **1**. In contrast, the impact of the TFP at position 8 on the overall geometry markedly differs from compounds **2** to **3**. Both pyridines do not face each other, resulting in a T-shaped conformation between the pyridine and naphthalene units and stabilizing interactions that contribute to the conformational stability of the receptors. Consequently, a twister-like shape is formed that is suitably configured to encapsulate anions within it for the three receptors. All receptors **1**, **2**, and **3** display

different sizes of their cavities, defined by the distances between the centroids of both TFP (8.2 Å, 7.3 Å, and 3.5 Å, respectively).

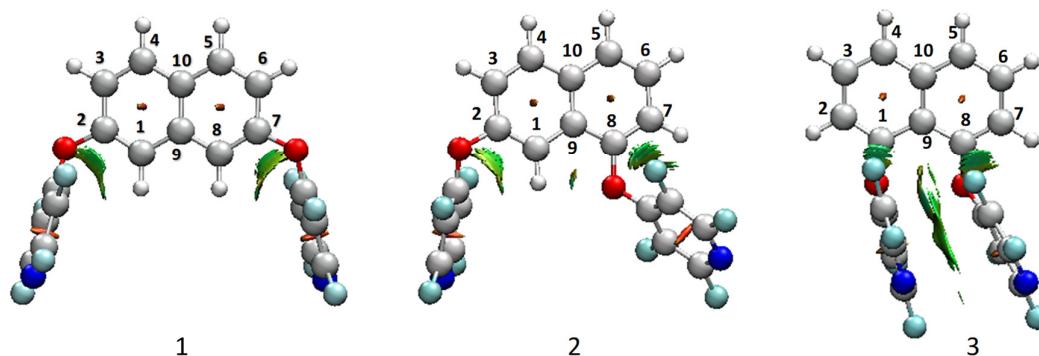


Figure 1. Optimized geometries' NCIPlot of **1**, **2** and **3** performed on multiwfn software.

Chloride-binding study:

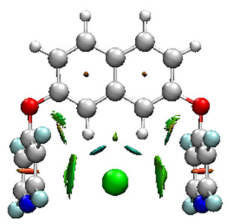
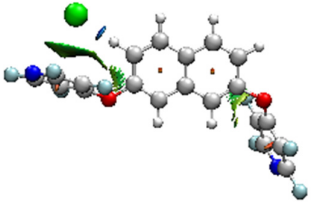
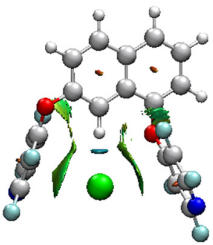
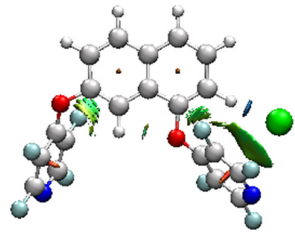
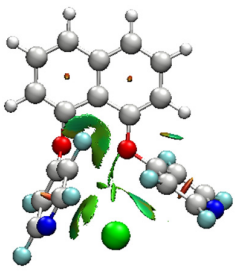
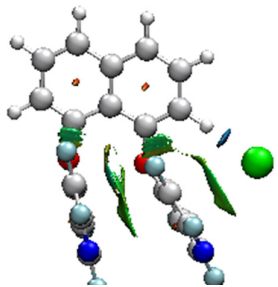
The preorganization of receptors **1-3**, resulting from the three-dimensional molecular arrangement and the relative positions of TFP and naphthalene, creates a cavity capable of hosting an anion. However, the anion can also position itself outside to interact with a single TFP. Therefore, multiple starting points were considered to determine the most stable and likely structures. All possibilities were optimized. Although all optimized complexes showed no imaginary frequencies indicating stable configurations, one complex for each receptor was more stable than the others. The most stable complex structures in the case of Cl⁻ inside and outside the cage, are represented in Table 1.

In the cases of receptors **1** and **2**, the most stable complexes (**[1a+Cl]⁻** and **[2a+Cl]⁻**) have the anion inside the cavities. The cavity sizes in **[1a+Cl]⁻** and **[2a+Cl]⁻** were slightly decreased (to 7.3 Å and 6.6 Å, respectively) to facilitate interactions between the chloride ion and both aromatic rings simultaneously. This allows the receptors to bind the chloride through two types of non-covalent interactions: C-H^{δ+}⋯Cl interaction and anion-π interactions as predicted by the NCIPlot calculations of the optimized geometries.

For receptor **3**, the cavity size in the complex **[3a+Cl]⁻** increased to 5.4 Å. The fluorinated pyridines repel each other, eliminating the original π-π stacking and enabling simultaneous anion-π interactions with the chloride ion. However, no C-H^{δ+}⋯Cl interactions are present in this configuration. **[3a+Cl]⁻** is not the most stable isomer. Instead, a chloride ion positioned outside the cavity, interacting with one TFP and forming a C-H^{δ+}⋯Cl interaction, results in the global minimum **[3b+Cl]⁻**. The cavity is too small in this case

for chloride being inserted in, and the stronger C-H \cdots Cl interaction provided by the naphthalene could explain why **[3b+Cl]⁻** is more stable than **[3a+Cl]⁻**.

Table 1 NCIPlot of the complexes optimized geometries studied in this work, performed on Multiwfn program.

	Cl ⁻ inside the cavity	Cl ⁻ outside the cavity	ΔE (kJ/mol)*
1	 [1a+Cl]⁻	 [1b+Cl]⁻	+24.0
2	 [2a+Cl]⁻	 [2b+Cl]⁻	+15.9
3	 [3a+Cl]⁻	 [3b+Cl]⁻	-30.5

* $\Delta E = E_{[Xb+Cl]^-} + ZPE_{[Xb+Cl]^-} - (E_{[Xa+Cl]^-} + ZPE_{[Xa+Cl]^-})$.

In the following section, only the complexes **[1a+Cl]⁻**, **[2a+Cl]⁻** and **[3b+Cl]⁻** are studied, being the more stable for each complex. The C-H_a bond length (Table 2) increases after the formation of the complexes **[1a+Cl]⁻** and **[2a+Cl]⁻**, indicative of a weak CH \cdots Cl bond. Moreover, it is observed that CH \cdots Cl distances are shorter than the sum of the Van der Waals radii for H and Cl (1.2Å and 2.11Å, respectively), suggesting that the two atoms are penetrating each other, thus interacting. Based on that, the penetration distances ($d_{\text{penetration}}$)^[9,11] of chloride and hydrogen atoms were calculated (Table 2). The $d_{\text{penetration}}$ in **[3b+Cl]⁻** is slightly greater than in **[2a+Cl]⁻**, which is itself greater than in **[1a+Cl]⁻**. This

indicates that the CH-Cl interaction in $[3b+Cl]^-$ may be stronger than in $[2a+Cl]^-$, and the latter is slightly more significant than in $[1a+Cl]^-$.

$d_{\text{penetration}}$ of the chloride with TFP^[11] (Table 2) shows a better anion- π interaction with $[3b+Cl]^-$ than with $[2a+Cl]^-$ and then with $[1a+Cl]^-$.

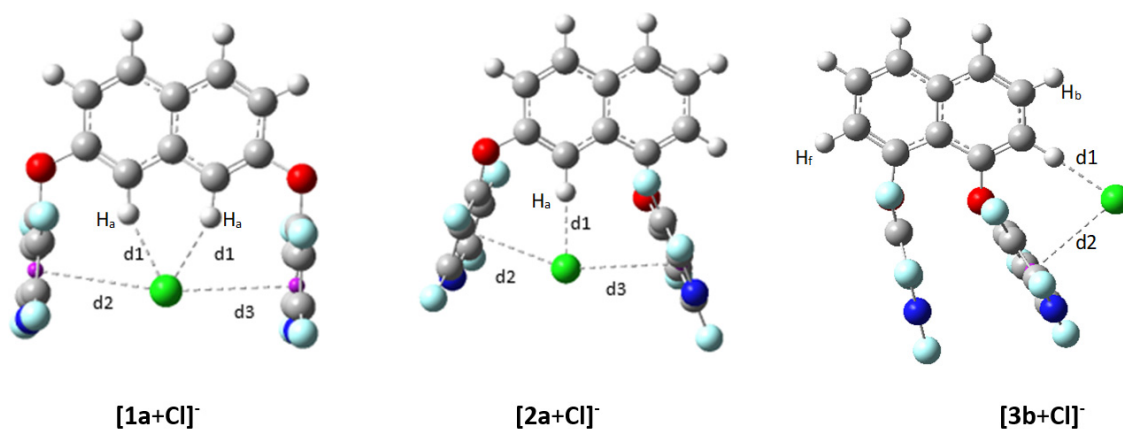


Figure 2. Optimized geometries of $[1a+Cl]^-$, $[2a+Cl]^-$ and $[3b+Cl]^-$. In purple: Centroids of TFP.

Table 2 distances in Å, $d_{\text{penetration}} = \sum dW_{\text{rad}ii} - 1/2(dx+dy)$, where $\sum vdW_{\text{rad}ii}$ is the sum of the van der Waals radii of carbon atom of the ring and chloride ion, and interaction energies.

	dC-H (in receptor)	dC-H (in complex)	dCH-Cl ⁻ (d ₁)	Centroid-Cl ⁻ (d ₂)	Centroid-Cl ⁻ (d ₃)	$d_{\text{penetration}}$ H-Cl	$d_{\text{penetration}}$ ring-Cl	$E_{\text{interaction}}$ *
								(kJ/mol)
$[1+Cl]^-$	1.09	1.10	2.35	3.7	3.7	0.96	0.11	-127.6
$[2+Cl]^-$	1.09	1.10	2.29	3.5	3.2	1.02	0.46	-118.1
$[3+Cl]^-$	1.09	1.11	2.19	3.2	-	1.12	0.61	-102.3

* $E_{\text{interaction}} = E_{\text{Complex}^-} - E_{\text{receptor}^-} - E_{\text{Chloride}}$.

Interaction energies: Comparison of the receptors' affinity to chloride ion

To compare the bonding strength within the complexes series, the interaction energies between the anion and each receptor were theoretically calculated in the gas phase, using the same level of theory and the global minimum for each complex. Receptor **1** displayed a stronger affinity for the chloride ion compared to receptor **2**, with interaction energies of -127.6 kJ/mol and -118.1 kJ/mol, respectively. Receptor **3** exhibited a lower interaction energy of -102.3 kJ/mol. This trend, despite the stronger interactions observed in $[3b+Cl]^-$ compared to $[2a+Cl]^-$ and $[1a+Cl]^-$, can be explained by two factors: firstly, the additivity and cooperativity of weak interactions provided by the cage structure and secondly, the fact that CH interactions are stronger than anion- π interactions ($[1a+Cl]^-$ has two CH interactions). This highlights the extent of the cooperative effect among weak interactions in stabilizing

the complex, as well as the multifunctional role of the naphthalene as a rigid spacer and a source of a complementary weak non-covalent interaction.

Importance of fluorine atoms:

Fluorine atoms, being electron-withdrawing, increase the acidity of the pyridines and thus facilitate the creation of the anion- π interaction^[12]. It is also important to study their effect on the overall design. In this context, non-fluorinated equivalents of receptors **1**, **2**, and **3**, as well as their corresponding complexes, were studied theoretically using DFT.

The geometry optimization of the three receptors (Figure 3) revealed distinct differences in the spatial arrangement of the pyridine rings in the absence of fluorine atoms. In receptor **4**, the pyridine rings are still face-to-face but no longer parallel. The nitrogen atoms are more distant, eliminating the cage-like preorganization effect. In receptor **5**, the pyridine rings are arranged face-to-side. Interestingly, in receptor **6**, the pyridine rings remain face-to-face and parallel.

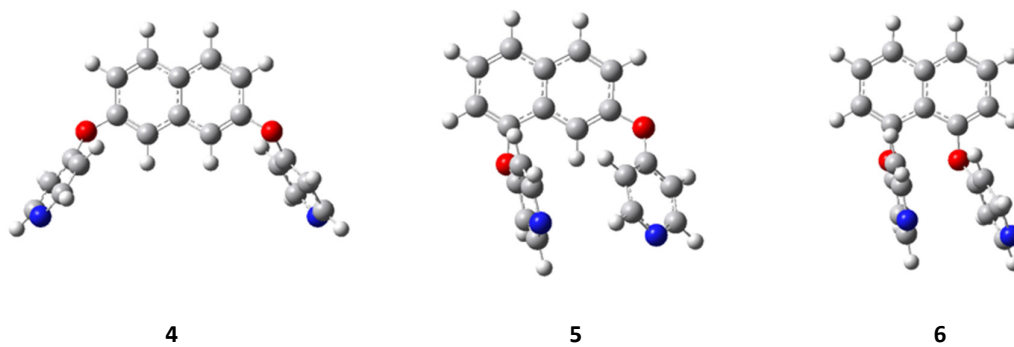


Figure 3. Optimized geometries of non-fluorinated receptors 4, 5 and 6.

NCIPlot analysis of the corresponding complexes (Figure 4) showed that the altered geometries result in different interaction patterns. Receptors **4** and **5** form a total of three CH-anion interactions (one with the naphthalene and one with each pyridine), whereas receptor **6** forms two CH-anion interactions (one with the naphthalene and one with a pyridine). None of the three complexes show an anion- π interactions, even for **[6+Cl]⁻**, despite its face-to-face pyridine arrangement.

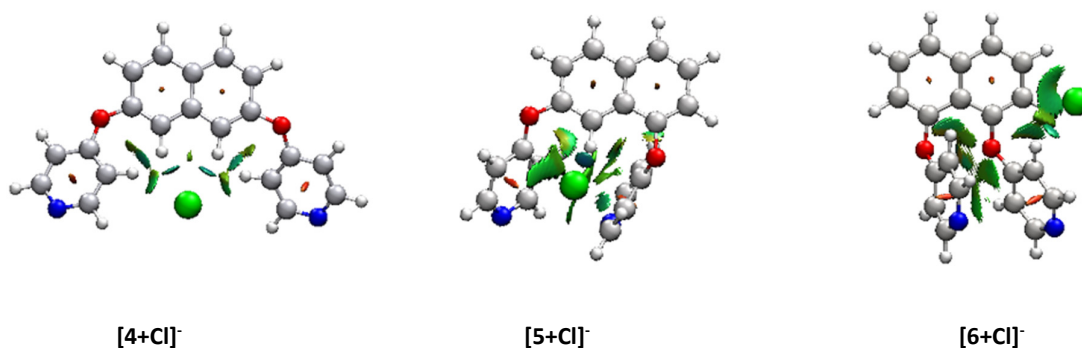


Figure 4. NCIPlot of non-fluorinated complexes performed on Multiwfn program.

The interaction energies with chloride anions are significantly lower for the non-fluorinated receptors compared to their fluorinated counterparts (see Table 3). Interestingly, there is an inversion of relative affinity: receptor **2** was more effective than receptor **3** in the fluorinated series, whereas receptor **6** is more effective than receptor **5** in the non-fluorinated series. Nonetheless, receptor **1** remains the most effective, and its non-fluorinated equivalent, receptor **4**, has a higher affinity than receptors **5** and **6**. By comparing the interaction energies, the cooperativity between anion- π and CH interactions appears to be superior to interactions involving only CH groups. Fluorine atoms are crucial not only for generating anion- π interactions but also for controlling the geometry of the complex. These findings highlight the crucial role of fluorine atoms in enhancing the binding efficiency and specificity of the receptors through geometric and electronic modifications.

Table 3 Interaction energies of non-fluorinated complexes.

	$E_{\text{interaction}}$ (kJ/mol)	$\Delta E_{\text{interaction}}$ (kJ/mol)*
[4+Cl] ⁻	-87.6	+40.0
[5+Cl] ⁻	-69.2	+48.9
[6+Cl] ⁻	-73.0	+29.3

* $\Delta E_{\text{interaction}} = E_{\text{interaction}}$ (fluorinated receptor) - $E_{\text{interaction}}$ (non-fluorinated receptor) for a receptor similar substitution pattern.

Synthesis:

The three receptors **1**, **2**, and **3** were synthesized in mild conditions, following the same procedure^[13]: nucleophilic aromatic substitution reaction in acetonitrile as solvent and K_2CO_3 as base at room temperature. (Figure 5)

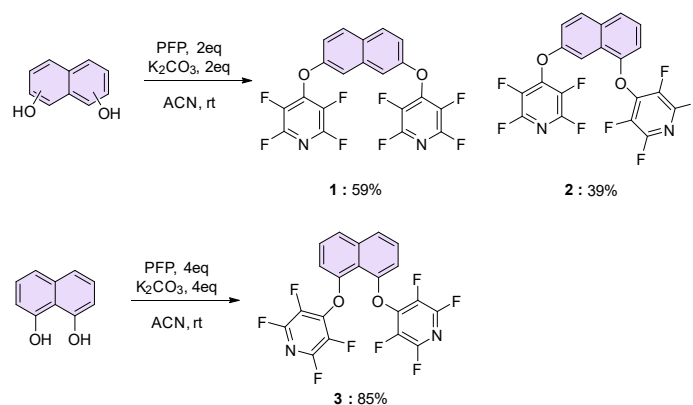


Figure 5. Synthesis routes of receptors **1**, **2**, and **3**.

The solid-state data confirm those obtained in the theoretical section for receptors **1** and **2**^[14]. Indeed, the X-ray crystallography confirmed the predicted structure of **1** and **2** (Figure 6), the overall topology of receptors, and the positions and orientations of the TFP groups. The latter form a well-defined and preorganized cavity able to host anions through anion- π and C-H-anion interactions. The cavity sizes of compounds **1** and **2**, as determined by X-ray crystallography, are 7.7 Å and 7.3 Å, respectively. The C-H distances in the naphthalene rings involved in interactions with chloride are 0.93 Å for compound **1** and 0.95 Å for compound **2**. All X-ray results are consistent with DFT calculations; the observed differences are within a small range of 0.5 Å for the cavity size of **2** and 0 Å for **2**, 0.17 Å and 0.14 Å for **1** and **2**, respectively, regarding the distances.

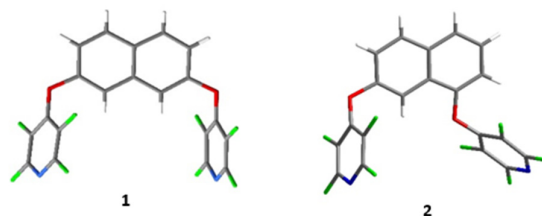


Figure 6. X-Ray crystallographic structure of **1** and **2**.

NMR titration analysis: To further explore the role of naphthalene as a C-H interaction donor, we conducted NMR titration experiments focusing on receptor **1**, which appears to form the most stable complex according to DFT calculations. When ongoing from 0 to 40 equivalents of TBACl, one observed the chemical shift of the H_a protons. Initially overlapping with part of the H_b proton signal as a broad singlet, H_a begins to appear as a doublet. It unshielded from 7.42 ppm to 7.46 ppm (Figure 7a). The other protons chemical shifts didn't change during the titration. The observed slight shift of H_a proton ($\Delta\delta = 0.04$ ppm) suggests the presence of a C- $H_a \cdots Cl$ bond. This interaction is much weaker than typical

hydrogen bonds, which typically show shifts between 2 and 3 ppm. To ensure that this shift was not due to the environment such as concentration or solvent effects, we performed a control experiment with *o*-dimethylnaphthalene under identical conditions (Figure 7b), which showed no such shift. Additionally, a ^{19}F NMR titration was conducted to detect potential anion- π interactions, but no significant shifts were observed (see Figure S18, supplementary Information). This confirms that while anion- π interactions are weak and challenging to detect in solution, the presence of tetrafluoropyridines (TFP) in the receptor is crucial for facilitating the C-H interactions, as evidenced by the changes observed in the proton NMR spectra.

These findings underline the cooperative role of TFP groups in enhancing the C-H interactions, which are absent when TFP are not present. This highlights the multifunctional capability of the naphthalene-based receptor, combining anion- π and C-H interactions to achieve selective chloride recognition.

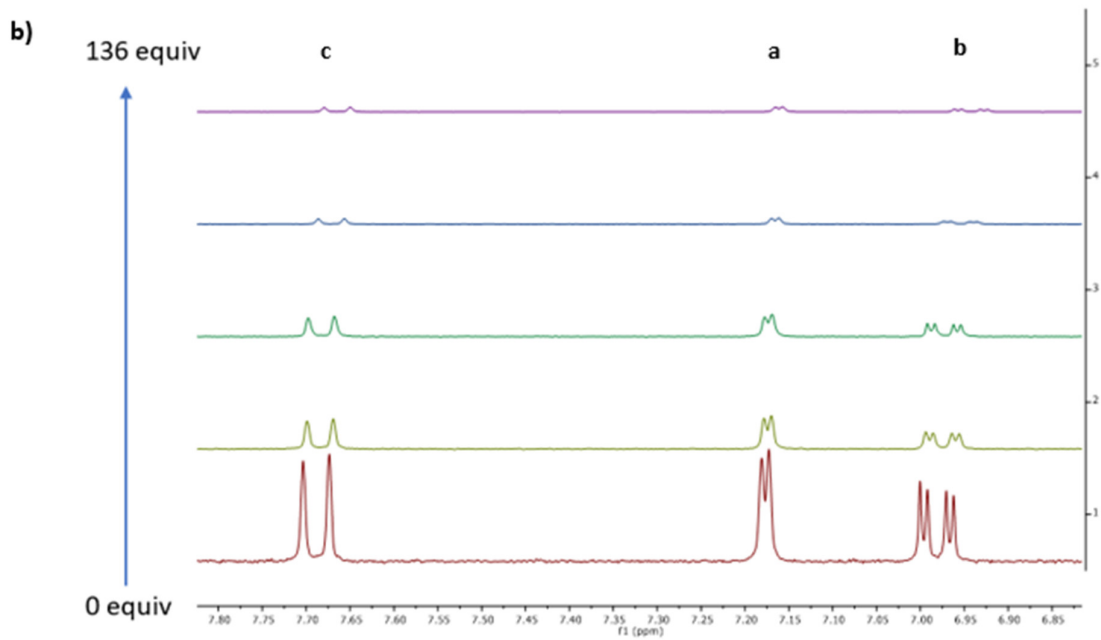
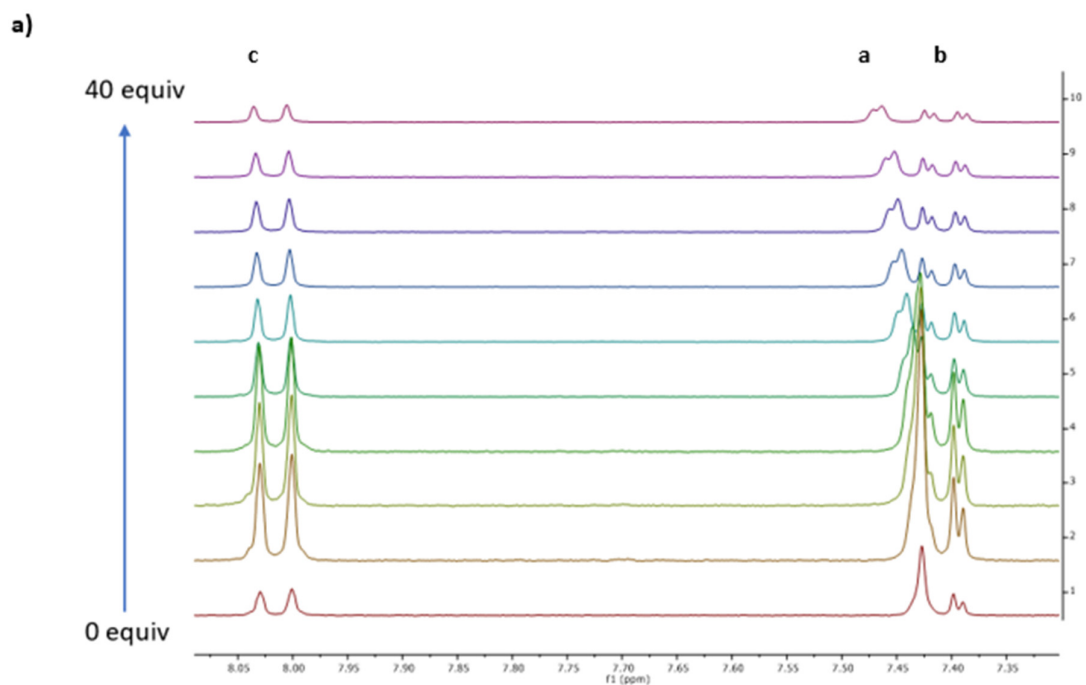
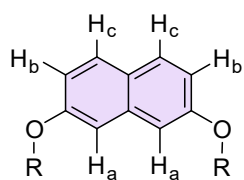


Figure 7. NMR ^1H titration in ACN-d_3 at $3.5 \cdot 10^{-3} \text{ M}$ of **a)** receptor **1** ($\text{R}=\text{TFP}$), **b)** *o*-dimethoxy-naphthalene ($\text{R}=\text{Me}$) with tetrabutylammonium chloride.

Mass spectrometry

ESI and CID experiments. Our theoretical study has demonstrated that these chloro complexes do correspond to stable species in the gas phase, although the computed interaction energies turn to be lower than those typically estimated for molecular receptors involving both hydrogen bond(s) and π -anion interactions^[15]. So, we decided to perform a mass spectrometry study in order to determine whether these complexes involving solely the doubly-substituted naphthalene motif could be actually observed experimentally. We initiated our study with a 3D ion trap instrument which gives us the possibility, if necessary, to perform MSⁿ experiments. Figure 8a presents an electrospray spectrum of an equimolar solution (10⁻⁴M) of **1**/NBu₄Cl prepared in a 90/10 ACN/water mixture. One can see that the base peak of the electrospray spectrum, detected at m/z 493, corresponds to the [**1**+Cl]⁻ complex, as attested by the characteristic isotopic distribution in agreement with the [C₂₀H₆O₂N₂F₈Cl] elemental composition, thereby conforming the stability of such complex in the gas phase. A complex with a 2:1 stoichiometry, [(**1**)₂+Cl]⁻, is also presently detected (m/z 951) at a lower intensity. Noticeably, this particular stoichiometry is observed neither with compound **2**, nor with compound **3** (see Figure S13a and S13b). In Figure 8a, one can also see a series of ions between m/z 250 and 350, detected at m/z 255, 283, 297, 311, 325 and 339. These ions correspond to a series of deprotonated fatty acids (C_nH_{2n+1}COO⁻, n=15,17-21), probably introduced during the purification step of the compounds. Although corresponding to trace amounts, they are characterized by a high ionization efficiency, hence a significant abundance. Furthermore, these contaminants are difficult to get rid of, and their intensity was slowly increasing as we went through the samples. Interestingly, these anions were also found to interact with the receptors, giving to a series of ions around m/z 750, as attested for example by the CID spectrum of the m/z 741 ion (Figure S14), which dissociates according to the loss of the intact receptor (458 u) to generate the m/z 283 ion.

Comparison of the extracted ion chromatogram intensity (EIC) of the 1:1 complex (Figure S13c) obtained for the three electrospray spectra, which were recorded exactly under the same experimental conditions, shows that the contribution to the total ion chromatogram (TIC) of the 1:1 complex is decreasing, ongoing from **1** (~43%), to **2** (~37 %) and then **3** (~18%), consistent with the decrease of the interaction energies. We have also studied the effect of the mixture composition onto the ESI spectrum. To this end, 1/1, 1/2, 2/1 mixtures of receptor/NBu₄Cl were prepared in a 90/10 ACN/water solution. Increasing the concentration of the receptor did not result in a more intense 2:1 complex. On the other hand, doubling the salt concentration is associated with the significant increase of the [NBu₄Cl+Cl]⁻ ion detected at m/z 312 and superimposed on fatty acid peaks.

In order to gain some insights about the structure of the 1:1 complexes, we recorded their MS/MS spectrum. To this end, the ions were mass-selected and subjected to collision induced dissociation

(CID) with helium inside the trap. The MS/MS spectrum of the $[1+Cl]^-$ complex is given in Figure 8b. Only one intense product ion is detected, at m/z 308. Unlike the complexes involving receptors with a urea motif^[4,15-17], deprotonation of the receptor associated with loss of HCl is presently not observed when using the ion trap. The same result is obtained with the two other receptors. The m/z 308 ion is associated with the elimination of a C_5F_4NCl moiety and the formation of $[C_{15}H_6O_2NF_4]^-$. A nucleophilic substitution (Scheme 1) may be assumed to account for the formation of m/z 308, which is coherent with the calculated structure (*vide supra*), in which the chloride is located inside the cavity and close to the carbon atoms undergoing the nucleophilic attack.

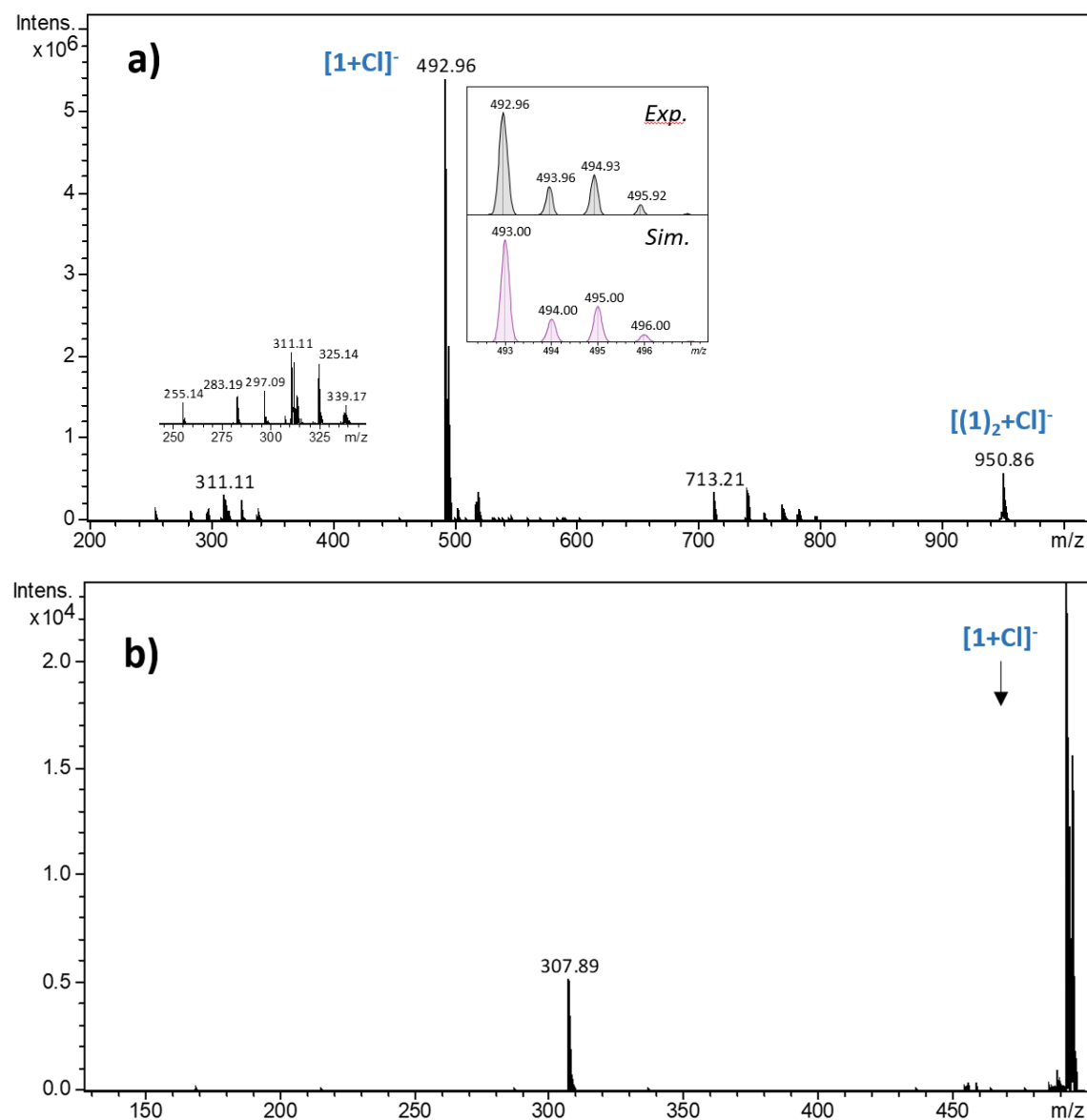
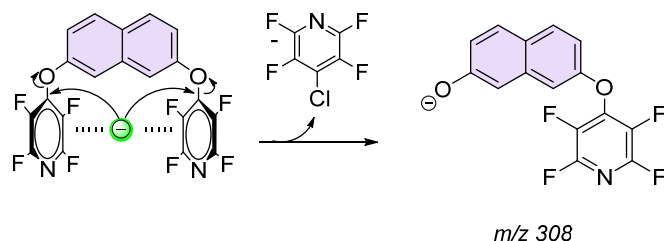


Figure 8. (a) Negative-ion electrospray mass spectrum of an equimolar mixture of $1/NBu_4Cl$ ($10^{-4}M$) in a 90/10 ACN/water solution, (b) MS/MS spectrum of the $[1 + Cl]^-$ ion (m/z 493-495), recorded on a 3D quadrupole ion trap.



Scheme 1 proposed mechanism for the formation of m/z 308.

MS3 experiments (not shown) allowed us recording the CID spectrum of m/z 308. It is characterized by the loss of HF (m/z 288) and the formation of an ion detected to m/z 166, which may be attributed to a TFP moiety $[C_5F_4NO]^-$, further supporting the structure postulated for m/z 308. In the case of receptor **1**, the CID spectrum of the 1:2 complex has also been recorded, and as expected the only dissociation channel observed is the loss of an intact receptor (458u; Figure S15).

The main drawback of the ion trap is that the low mass range of the CID spectra is limited by the low mass cutoff of 27% of the precursor ion. This means that for the 1:1 complex, possible product ions below m/z 133, and more especially the eventual elimination of the intact receptor leading to Cl^- (m/z 35/37), cannot be observed. So, we also recorded the CID spectra of the complexes onto a Q-TOF instrument (Xevo, Waters; see supporting information for the experimental conditions). A typical MS/MS spectrum, obtained for the complex $[1+Cl]^-$ is given in Figure S16. These MS/MS spectra turned to be somewhat different from that recorded with the ion trap, as they present additional product ions. This is not necessarily surprising as the experimental conditions to record the MS/MS spectra are sensibly different, the most noticeable difference being the collision gas, since argon is employed in the Q-TOF instead of helium in the 3D trap. Consequently, the amount of internal energy transferred to the precursor ion during collisional excitation is probably different and higher during Q-TOF MS/MS experiments. For the three complexes, the same set of product ions are observed. First, the dominant process is the elimination of the intact receptor leading to chloride (Cl^- ; m/z 35), that could not be observed on the ion trap. Remarkably, the deprotonated receptor is detected in significant abundance (m/z 457), through elimination of HCl, the associated proton coming necessarily from the naphthalene moiety. Note that the deprotonation is observed for the three complexes. This may suggest that for the receptor **3**, Cl^- could be located outside the cavity and interact with only one pyridine ring. Like in Figure 8b, we do observe the formation of the m/z 308 ion by loss of C_5F_4NCl , which further dissociates by elimination of HF, as previously observed during MS3 experiments (*vide supra*). Finally, note that at higher collision energy, the formation of $[C_5F_4NO]^-$ (m/z 166), is also detected, but in weak amounts.

Survival yield experiments We also used the Q-TOF instrument to record the MS/MS spectra of the three complexes at different collision energies, and for each collision energy, we calculated the intensity of the remaining precursor ions. We employed a survival yield methodology^[5,18,19], which is commonly used in mass spectrometry to qualitatively assess the stability of precursor ions. To this end, the collision energy was gradually increased (Figure 9). At each value of the collision energy, the ratio of the intact complex to its fragments is measured, to ultimately estimate the collision energy (CE50) needed to achieve the dissociation of 50 % (SY=0.5) of the complex. As the three complexes presently studied are isobaric, we decided to remain in the laboratory frame and did not calculate center of mass collision energies. For each system, experiments were repeated three times. Figure 9 clearly shows that higher values of collision energy are needed for **[1+Cl]⁻**, to achieve 50 % of fragmentation.

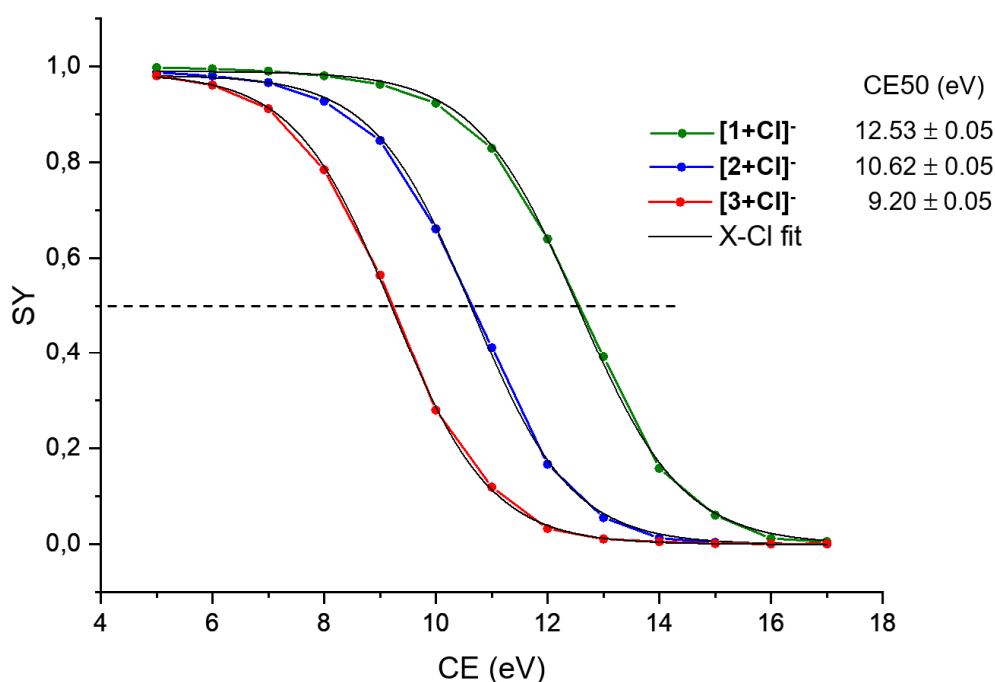


Figure 9. Plot of the decreasing intensity of the complexes (survival yield, SY) against the increasing collision energy. **[1+Cl]⁻** in green, **[2+Cl]⁻** in blue and **[3+Cl]⁻** in red. A sigmoidal fit function is applied in black (SLogistic1, R²>0.999). The SY corresponds to the average of triplicate measurements. Product ions considered to obtain these traces: m/z 35, 166, 288, 308 and 457.

The determined CE50 values given in Figure 9 indicate that the complex **[1+Cl]⁻** is more stable **[2+Cl]⁻**, **[3+Cl]⁻** being the least stable of the series. This ordering demonstrates that the binding strength of receptor **1** towards chloride is higher than **2**, receptor **3** exhibiting the weakest affinity towards Cl⁻ of this series. This experimental finding is therefore in agreement with our DFT predictions.

Ion mobility. To complete this mass spectrometry study, we also performed some ion mobility (IMS) experiments. To this end, we used our recently installed Select Series Cyclic-IMS QToF (Waters) mass

spectrometer^[20,21]. This instrument is equipped with a cyclic ion mobility (cIM) device, which allows the resolution R of the IMS separation to be improved, by increasing the number of passes a selected precursor ion can perform inside the ion mobility ring, thereby virtually increasing the length of the ion mobility cell. The R term scales as $\sim 65\sqrt{n}$, where n is the number of passes. In a seminal paper^[20], an example of isomer separation by increasing the resolution R is given for two the protonated peptides SDGRG and GRGDS at m/z 491.2 (that is with a m/z value similar to those of the complexes presently studied), and they showed these two isobaric ions could be easily separated by cIMS, by increasing the number of passes. We tried to record the ion mobilogram of the three complexes. If one considers for example receptors **1** and **3**, the structures of the global minima are predicted to be different as Cl^- is in between the pyridine rings for the former, and interacts with only one pyridine for the latter. One might expect that the two complexes have a slightly different collision cross section (CCS) and hence could be differentiated by measuring their arrival time. The mobilograms obtained for both $[\mathbf{1}+\text{Cl}]^-$ and $[\mathbf{3}+\text{Cl}]^-$ after a single pass inside the ion mobility cell and recorded separately under the same conditions, are given in Figure S17. The arrival times measured are short (13.5 ms, which is not surprising given the small size of these systems) and are similar for the two ions, suggesting that they would have similar collision cross sections in spite of a theoretical different spatial organization and chloride location. One can also see that for both complexes, the mobilogram exhibits a single peak with a narrow gaussian shape. The fact that the trace is rather narrow and symmetric, and that increasing the number of passes the ions undergo within the cyclic mobility cell (up to $n=10$), did not result in any peak broadening or peak splitting, may suggest a single population of ions for each complex. However, a mixture of two forms having very close CCSs cannot be rigorously discarded since a difference of less than 0.5 % in CCS may require a resolving power higher than 300^[22], that is a number of cycles $n \gg 10$. However, it is worth mentioning that the ionic signal decreases progressively as one increases the number of passes within the cyclic cell, and that with these particular systems we managed to increase n only up to 14, insufficient to reach these R values.

Conclusion

This study demonstrates the effective use of multifunctional naphthalene-based receptors for chloride recognition through cooperative anion- π and C-H \cdots Cl interactions. By strategically modifying the substitution patterns of tetrafluoropyridines (TFP) on a rigid naphthalene spacer, we achieved tunable cavity sizes and enhanced interaction properties. Theoretical studies using Density Functional Theory (DFT) provided insights into the optimal geometries and predicted the chloride binding capabilities of the receptors. Experimental validation via X-ray crystallography confirmed the preorganized structures

capable of hosting anions. NMR titration experiments highlighted the presence and importance of C-H \cdots Cl interactions facilitated by TFP groups, which are crucial for the receptors' functionality. Mass spectrometry analyses further supported the stability and binding efficacy of the chloride complexes in the gas phase.

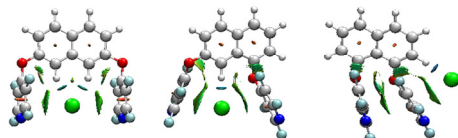
The combination of these analytical tools underlines the importance of the preorganized cage structures, the role of naphthalene as a rigid spacer and source of complementary non-covalent interactions, and the cooperative effect of weak interactions in enhancing the binding affinity and efficiency of the receptors. The strategic design of the substitution position significantly impacts the interaction efficiency with chloride ion, highlighting its critical role. This comprehensive approach provides a robust framework for designing effective anion receptors for various applications.

Supporting Information

The authors have cited additional references within the Supporting Information.^[23-29] The Supporting Information includes experimental procedures, mass spectrometry analysis, NMR, mass spectra, ¹⁹F NMR titration spectra and computational results.

TOC:

Cooperativity between CH \cdots Cl and Cl \cdots π interactions



This article focuses on developing efficient receptors for chloride. A series of novel receptors based on a rigid naphthalene spacer bearing tetrafluoropyridines (TFPs) in various substitution patterns have been synthesized. Their complexation efficiencies are essentially studied in the gas phase through mass spectrometry experiments. DFT calculations and NMR titration were also performed.

Aknowledgments

We are grateful to the CNRS and the Universities of Versailles Saint Quentin, Evry and Paris-Saclay. OZ and JH thank the French Ministère de l'Enseignement Supérieur et de la Recherche for PhD funding. We thank Genopole® (Evry, France) for providing financial support for the acquisition of the cyclic ion mobility instrument. We also thank the University of Evry Paris-Saclay for its financial contribution to the acquisition of the ion mobility instrument (program MaSTeR). This work was also supported by the french National Research Agency under the programm CHARMMMAT ANR-11-LABX-0039 grant for the acquisition of the 3D ion trap instrument.

This work was performed using HPC resources from the "Mésocentre" computing center of CentraleSupélec Paris-Saclay and École Normale Supérieure Paris-Saclay supported by the CNRS and the Région Île-de France (<http://mesocentre.centralesupelec.fr/>).

Conflict of Interest:

The authors declare no conflict of interest.

References

- [1] P. A. Gale, E. N. W. Howe, X. Wu, M. J. Spooner, *Coord. Chem. Rev.* **2018**, *375*, 333–372.
- [2] L. Chen, S. N. Berry, X. Wu, E. N. W. Howe, P. A. Gale, *Chem* **2020**, *6*, 61–141.
- [3] N. Busschaert, C. Caltagirone, W. Van Rossom, P. A. Gale, *Chem. Rev.* **2015**, *115*, 8038–8155.
- [4] R. Plais, G. Gouarin, A. Gaucher, V. Haldys, A. Brosseau, G. Clavier, J. Salpin, D. Prim, *ChemPhysChem* **2020**, *21*, 1249–1257.
- [5] M. Göth, F. Witte, M. Quennet, P. Jungk, G. Podolan, D. Lentz, W. Hoffmann, K. Pagel, H. Reissig, B. Paulus, C. A. Schalley, *Chem. – Eur. J.* **2018**, *24*, 12879–12889.
- [6] S. Kubik, C. Reyheller, S. Stüwe, *J. Incl. Phenom. Macrocycl. Chem.* **2005**, *52*, 137–187.
- [7] X. Wu, A. M. Gilchrist, P. A. Gale, *Chem* **2020**, *6*, 1296–1309.
- [8] M. Giese, M. Albrecht, K. Rissanen, *Chem. Rev.* **2015**, *115*, 8867–8895.
- [9] A. Frontera, P. Gamez, M. Mascal, T. J. Mooibroek, J. Reedijk, *Angew. Chem. Int. Ed.* **2011**, *50*, 9564–9583.
- [10] A. Frontera, D. Quiñonero, P. M. Deyà, *WIREs Comput. Mol. Sci.* **2011**, *1*, 440–459.
- [11] Y.-Z. Liu, K. Yuan, L. Liu, Z. Yuan, Y.-C. Zhu, *J. Phys. Chem. A* **2017**, *121*, 892–900.
- [12] I. Alkorta, I. Rozas, J. Elguero, *J. Am. Chem. Soc.* **2002**, *124*, 8593–8598.
- [13] W. D. G. Brittain, S. L. Cobb, *Org. Biomol. Chem.* **2019**, *17*, 2110–2115.
- [14] Deposition numbers
<urlhref="https://www.ccdc.cam.ac.uk/services/structures?id=doi:10.1002/cplu.202400380">
CCDC2360170 (for **1**), CCDC2360171 (for **2**), contain the supplementary crystallographic data
for this paper. These data are provided free of charge by the joint Cambridge Crystallographic
Data Centre and Fachinformationszentrum Karlsruhe
<urlhref="http://www.ccdc.cam.ac.uk/structures"> Access Structures service.
- [15] O. Zayene, R. Plais, L. Rolhion, F. Bourdreux, G. Pieters, A. Gaucher, G. Clavier, A. Coeuret, J.-Y. Salpin, D. Prim, *ChemistrySelect* **2024**, *9*, e202302763 (1-11).
- [16] R. Plais, G. Gouarin, A. Bournier, O. Zayene, V. Mussard, F. Bourdreux, J. Marrot, A. Brosseau, A. Gaucher, G. Clavier, J.-Y. Salpin, D. Prim, *ChemPhysChem* **2023**, *24*, e202200524.
- [17] R. Plais, H. Boufroura, G. Gouarin, A. Gaucher, V. Haldys, A. Brosseau, G. Clavier, J.-Y. Salpin, D. Prim, *RSC Adv.* **2021**, *11*, 9476–9487.
- [18] A. Memboeuf, A. Nasioudis, S. Indelicato, F. Pollreis, Á. Kuki, S. Kéki, O. F. Van Den Brink, K. Vékey, L. Drahos, *Anal. Chem.* **2010**, *82*, 2294–2302.
- [19] T. M. Kertesz, L. H. Hall, D. W. Hill, D. F. Grant, *J. Am. Soc. Mass Spectrom.* **2009**, *20*, 1759–1767.
- [20] K. Giles, J. Ujma, J. Wildgoose, S. Pringle, K. Richardson, D. Langridge, M. Green, *Anal. Chem.* **2019**, *91*, 8564–8573.
- [21] N. Tomczyk, K. Giles, K. Richardson, J. Ujma, M. Palmer, P. K. Nielsen, K. F. Haselmann, *Anal. Chem.* **2021**, *93*, 16379–16384.
- [22] J. N. Dodds, J. C. May, J. A. McLean, *Anal. Chem.* **2017**, *89*, 952–959.
- [23] H. E. Gottlieb, V. Kotlyar, A. Nudelman, *J. Org. Chem.* **1997**, *62*, 7512–7515.
- [24] G. M. Sheldrick, *Acta Crystallogr. Sect. Found. Adv.* **2015**, *71*, 3–8.
- [25] G. M. Sheldrick, *Acta Crystallogr. Sect. C Struct. Chem.* **2015**, *71*, 3–8.
- [26] O. V. Dolomanov, L. J. Bourhis, R. J. Gildea, J. A. K. Howard, H. Puschmann, *J. Appl. Crystallogr.* **2009**, *42*, 339–341.
- [27] J. Contreras-García, E. R. Johnson, S. Keinan, R. Chaudret, J.-P. Piquemal, D. N. Beratan, W. Yang, *J. Chem. Theory Comput.* **2011**, *7*, 625–632.
- [28] H. S. Rzepa, <https://www.ch.ic.ac.uk/rzepa/cub2nci/>.
- [29] E. F. Pettersen, T. D. Goddard, C. C. Huang, G. S. Couch, D. M. Greenblatt, E. C. Meng, T. E. Ferrin, *J. Comput. Chem.* **2004**, *25*, 1605–1612.

Table of content

1. General procedures, Material and Instrumentation.....	3
1.1..... General experimental procedures and Materials	3
1.2..... Instrumentation	3
1.3 Molecular modelling and software	4
2. Synthetic procedures	6
3. Mass spectrometry analysis:	15
4. NMR titration	18
.....	18
5. DFT Analysis:	19
5.1 Energies interactions calculation:.....	19
5.2 Coordinates and thermodynamics data of 1	20
5.3 Coordinates and thermodynamics data of [1a+Cl] ⁻	21
5.4 Coordinates and thermodynamics data of [1b+Cl] ⁻	22
5.5 Coordinates and thermodynamics data of 2	23
5.6 Coordinates and thermodynamics data of [2a+Cl] ⁻	24
5.7 Coordinates and thermodynamics data of [2b+Cl] ⁻	25
5.8 Coordinates and thermodynamics data of 3	26
5.9 Coordinates and thermodynamics data of [3a+Cl] ⁻	27
5.10 Coordinates and thermodynamics data of [3b+Cl] ⁻	28
5.11 Coordinates and thermodynamics data of 4	29
5.12 Coordinates and thermodynamics data of [4+Cl] ⁻	30
5.13 Coordinates and thermodynamics data of 5	31
5.14 Coordinates and thermodynamics data of [5+Cl] ⁻	32
5.15 Coordinates and thermodynamics data of 6	33
5.16 Coordinates and thermodynamics data of [6+Cl] ⁻	34

Table of illustrations

Figure S1. ¹ H NMR spectrum of 1	7
Figure S2. ¹⁹ F NMR spectrum of 1	7
Figure S3. ¹³ C NMR spetrum of 1	8
Figure S4. High resolution mass spectrum of 1	8
Figure S5. ¹ H NMR spectrum of 2	9
Figure S6. ¹⁹ F NMR spectrum of 2	10

Figure S7. ^{13}C NMR spectrum of 2	10
Figure S8. High resolution mass spectrum of 2	11
Figure S9. ^1H NMR spectrum of 3	13
figure S10 ^{19}F NMR spectrum of 3	13
Figure S11. ^{13}C NMR spectrum of 3	14
Figure S12. High resolution mass spectrum of 3	14
Figure S13. Electrospray mass spectrum of an equimolar (10^{-4} M) mixture of a) 2/NBu₄Cl b) 3/NBu₄. c) Total ion current (TIC) and extracted ion chromatogram (EIC) of [n+Cl]⁻ ion for the different mixtures. Experiments performed on the AMAZON SPEED ETD ion trap	15
figure S14. CID mass spectrum of the m/z 741 ion recorded on the AMAZON SPEED ETD ion trap. ...	16
figure S15. CID mass spectrum of the ion [(1)2+Cl] ⁻ (m/z 951) recorded on the AMAZON SPEED ETD ion trap	16
figure S16. CID mass spectrum of the ion [1+Cl] ⁻ (m/z 493), recorded with the XEVO QTOF instrument (waters) at a collision energy of 14 eV (laboratory frame). Mass selection : 493.0 ± 1.0 . The peak involving the ^{37}Cl atom (m/z 495) is presently not selected.	17
figure S17. Ion mobility mobilograms recorded for a) the ion [1+Cl] and b) the ion [3+Cl] ⁻ -after a single pass within the cyclic mobility cell	18
figure S18. NMR ^{19}F titration in ACN-d ₃ at $3.5 \cdot 10^{-3}$ M of 1 with tetrabutylammonium chloride	18

1. General procedures, Material and Instrumentation

1.1 General experimental procedures and Materials

Unless otherwise noted, all starting materials were obtained from commercial suppliers and used without purifications.

Reaction progress was carried out using pre-coated TLC sheets ALUGRAM® Xtra SIL G/UV₂₅₄ (0.20mm) from Macherey-Nagel® and visualized under 254 and 365 nm UV lamp from Fisher Bioblock Scientific®. Flash chromatography was proceeded using Silica 60M (0.04-0.063mm) for column chromatography silica gel from Macherey-Nagel®.

1.2 Instrumentation

¹H NMR spectra were recorded with Bruker AV-I 300MHz spectrometer at 298K, referenced to TMS signal and were calibrated using residual proton in Acetone d₆ (δ =2.05ppm), according to the literature.^[1] ¹⁹F NMR spectra were recorded with Bruker AV-I 300MHz spectrometer at 282MHz and 298K and were calibrated using CFCl₃ as reference. ¹³C NMR spectra were recorded with a Bruker AV-I 300MHz spectrometer at 75MHz and 298 K and were calibrated using Acetone d₆ (δ = 29.8 ppm).^[1] ¹H NMR spectroscopic data are reported as follow: chemical shift δ [parts per million] (multiplicity, coupling constants in Hertz, integration). Multiplicities are reported as follow: s = singlet, d = doublet, t = triplet, q = quadruplet, quint = quintuplet, sext = sextuplet, hept = heptuplet, dd = doublet of doublet, td = triplet of doublet, tt = triplet of triplet, ddd = doublet of doublet of doublet, m = multiplet. ¹³C NMR spectroscopic data are reported in terms of chemical shifts δ [ppm] and when it is necessary multiplicity and coupling constant in Hertz.

Crystal data collection: Bruker APEX2; cell refinement: SAINT V8.40B (Brücker, 2016); data reduction: SAINT V8.40B (Brücker, 2016); program(s) used to solve structure: SHELXT^[2]; program(s) used to refine structure: SHELXL 2019/3^[3]; molecular graphics: Olex2 1.5^[4]; software used to prepare material for publication: Olex2 1.5^[4].

To check the structure of the product obtained during the synthesis, high resolution mass spectra (HRMS) were obtained with a Xevo QTOF instrument coupled to an electrospray ionization source (ESI-) (Waters Co., Milford, MA, USA, USA), using Leucine Enkephaline solution as internal calibrant.

Studies of the gas-phase interactions of **1**, **2** and **3** with chloride ion, were performed onto a 3D ion trap instrument (Bruker Amazon Speed ETD). Complexes were generated in the gas phase by electrospray ionization. To this end, equimolar mixtures of **2**/NBu₄Cl and **3**/NBu₄Cl were prepared. Starting from 5 10⁻² M stock solutions of **1**, **2** and **3** and NBu₄Cl solubilized in acetonitrile (ACN) and purified water, respectively, 10⁻⁴ M or 10⁻⁵ M mixtures of **2**/ NBu₄Cl and **3**/NBu₄Cl (90/10 ACN/H₂O) were introduced in the electrospray source by a syringe pump (4-5 μ L/min). Typical experimental conditions were as followed: Capillary voltage: - 4500 V; End plate offset: -500 V; Dry gas: 10 L/min / Dry gas temperature: 200 °C, Nebulizer gas: 7.3 PSI; Cap exit and Trap drive values automatically adjusted through the target mass parameter: 550 and 1025 to study the monomers and dimers, respectively.

All spectra were recorded in the "Maximum Resolution mode"

MS analysis: ICC mode: "on" (80000 ions) and acquisition time: auto.

MSⁿ analysis: ICC mode off / accumulation time 1 to 5 ms to reach c.a. 20000 ions for the selected precursor ion/ Isolation window 4 to 8 Da / Fragmentation delay 40 ms/ amplitude of fragmentation: 0.20-0.5 depending on the ions / Low mass cutoff: Auto (excepted where indicated).

The survival yields of [M+Cl]⁻ complexes were measured by mass spectrometry as follows: the instrument used is a quadrupole-time-of-flight high-resolution mass spectrometer Xevo QToF MS (Waters Co., Milford, MA, USA). Typical instrument parameters are as follows: infusion flow rate: 10 µL/min; source temperature: 120 °C; capillary voltage: 1.0 kV; sample cone voltage: 10 V; extraction cone: 2 V; nebulizer gas pressure: 6.5 bar; desolvation gas flow: 800 L/h; desolvation temperature: 500 °C. The capillary voltage and sample cone voltage were optimized for maximum abundance of the desired [M+Cl]⁻ complex. CID experiments were employed for MS/MS experiments using Ar as the collision gas. Complex ions of interest were *m/z*-selected in the quadrupole and fragmented in the collision cell with increasing collision energies from 5 to 17 eV.

For the cyclic mobility experiments, similar mass selection parameters were used. We also optimized the various parameters:

- ESI lockspray parameters: infusion flow rate: 4 µL/min; source temperature: 100 °C; capillary voltage: 3.5 kV; sample cone voltage: 50 V; nebulizer gas pressure: 5.0 bar; desolvation gas flow: 500 L/h; desolvation temperature: 250 °C.
- TWaves array parameters: cyclic TW velocity : 150 m/s ; Array TW velocity: 100 m/s; TW static height: 0V; TW ramp start height: 15V; TW ramp end height: 25V; TW ramping rate: 2.5 V/ms.

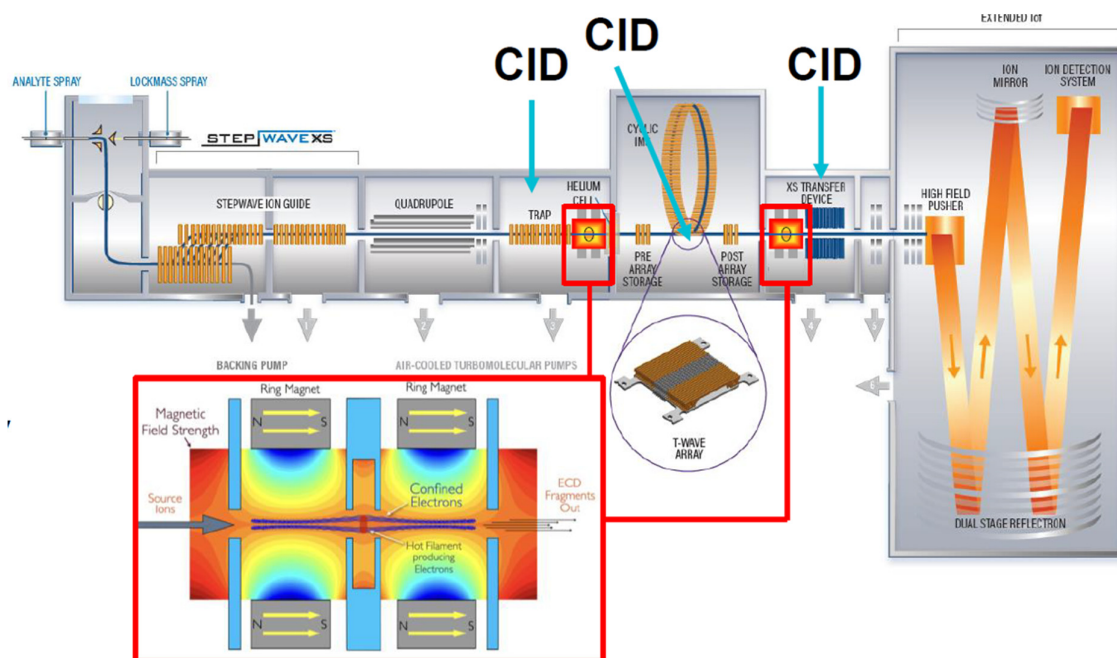


Figure S1: Schema of the cyclic IMS

1.3 Molecular modelling and software

All calculations were carried out using Gaussian 16® program:

Gaussian 16, Revision B.01, M. J. Frisch, G. W. Trucks, H. B. Schlegel, G. E. Scuseria, M. A. Robb, J. R. Cheeseman, G. Scalmani, V. Barone, G. A. Petersson, H. Nakatsuji, X. Li, M. Caricato, A. V. Marenich, J. Bloino, B. G. Janesko, R. Gomperts, B. Mennucci, H. P. Hratchian, J. V. Ortiz, A. F. Izmaylov, J. L. Sonnenberg, D. Williams-Young, F. Ding, F.

Lipparini, F. Egidi, J. Goings, B. Peng, A. Petrone, T. Henderson, D. Ranasinghe, V. G. Zakrzewski, J. Gao, N. Rega, G. Zheng, W. Liang, M. Hada, M. Ehara, K. Toyota, R. Fukuda, J. Hasegawa, M. Ishida, T. Nakajima, Y. Honda, O. Kitao, H. Nakai, T. Vreven, K. Throssell, J. A. Montgomery, Jr., J. E. Peralta, F. Ogliaro, M. J. Bearpark, J. J. Heyd, E. N. Brothers, K. N. Kudin, V. N. Staroverov, T. A. Keith, R. Kobayashi, J. Normand, K. Raghavachari, A. P. Rendell, J. C. Burant, S. S. Iyengar, J. Tomasi, M. Cossi, J. M. Millam, M. Klene, C. Adamo, R. Cammi, J. W. Ochterski, R. L. Martin, K. Morokuma, O. Farkas, J. B. Foresman, and D. J. Fox, *Gaussian, Inc., Wallingford CT, 2016*.

This work was performed using HPC resources from the “Mésocentre” computing center of CentraleSupélec and École Normale Supérieure Paris-Saclay supported by CNRS and Région Île-deFrance (<http://mesocentre.centralesupelec.fr/>).

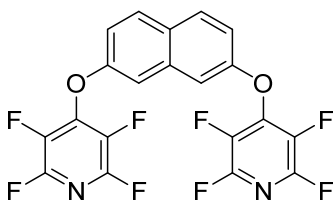
Computed structures were preoptimized with a MM2 forcefield using Chem3D[®]. Then, optimizations were calculated at APFD/aug-cc-pVDZ calculation level using Gaussian 16[®] software without any solvent correction. Stationary points were verified by a harmonic vibrational frequencies’ calculation. None of the predicated geometry has any imaginary frequency implying that the optimized geometry of each of the molecules under study lay at a minimum local point on the potential energy surface.

NCIplots were generated from total densities using the script developed by Rzepa available on the website application of the Imperial College London.^[5,6]

Distances were measured using Gaussview software on structures optimized without any solvent correction. Distances between tetrafluoropyridine centroid (defined using the six atoms of the tetrafluoropyridine rings) and chloride were measured using UCSF Chimera software.^[7]

2. Synthetic procedures

General procedure for 1 and 2: naphthalene-diol derivative (100mg, 0.6mmol) and K_2CO_3 were added to a round bottom flask. Pentafluoropyridine (211mg, 2eq) and 3 mL of acetonitrile were added under argon atmosphere. The mixture was stirred at room temperature overnight. The mixture was diluted with OEtAc (15mL) and washed with water (3x10mL) and Brine (20mL). The Crude was dried over $MgSO_4$ and vacuumed. The crude was purified over column chromatography.



1

Purification conditions: Petroleum ether/Ethyl acetate 98/2

Aspect: white solid

Yield: 59%

1H NMR (MHz, Acetone $\delta 6$, TMS): δ (ppm) : 8.09 (d, 2H, $^3J_{H-H}$ = 7.9 Hz), 7.61 (d, 2H, $^4J_{H-H}$ = 2.68 Hz), 7.52 (dd, 2H, $^4J_{H-H}$ = 2.44 Hz, $^3J_{H-H}$ = 9.08 Hz)

^{19}F NMR (282 MHz, Acetone $\delta 6$, $CFCl_3$): δ (ppm) -90.2 (m, 4F), -154.8 (m, 4F).

^{13}C NMR (75 MHz, Acetone $\delta 6$, TMS): δ (ppm): 155.8, 146.4-143.2 (large d, m, 2C $^1J_{C-F}$ = 240.1 Hz), 144.7 (m, 2C), 139.6-135.7 (large d, m $^1J_{C-F}$ =259.7 Hz) 135.7, 131.6, 129.1, 117.7 112.3.

Rf: 0.3

HRMS (ESI(-)/Q-TOF) m/z [M-H]⁻: calculated for: 457.0223 found: 457.0217

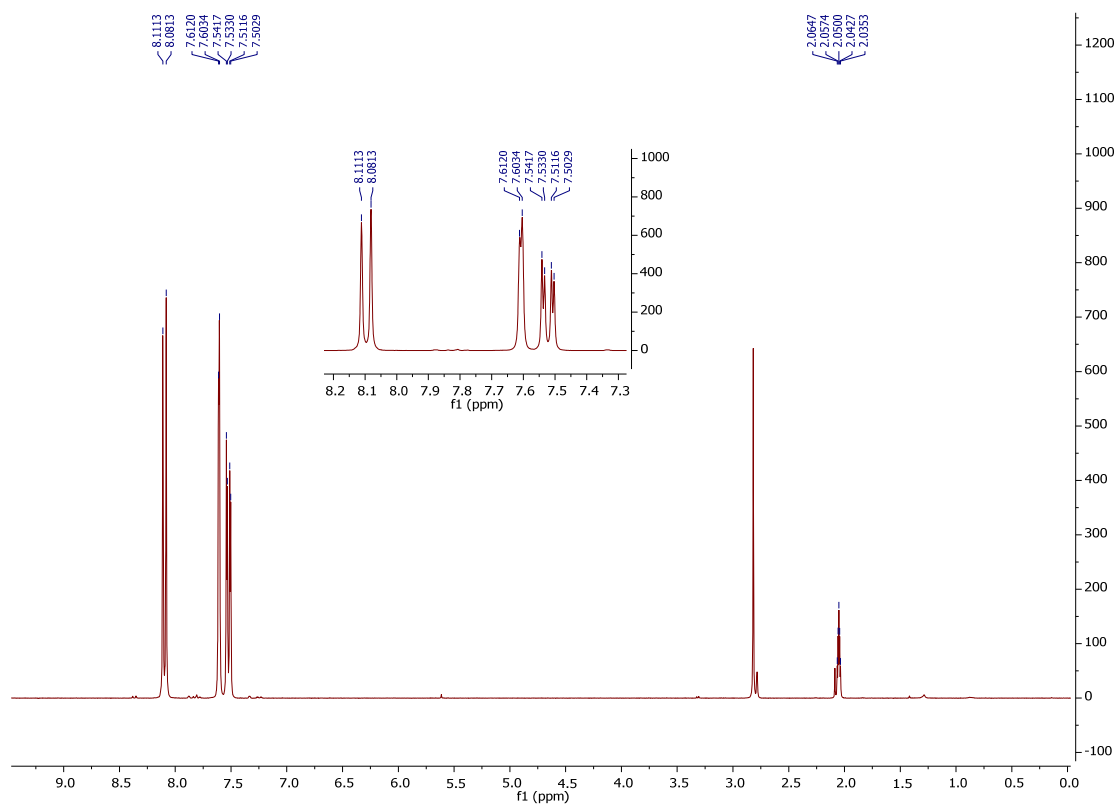


Figure S1. ^1H NMR spectrum of **1**

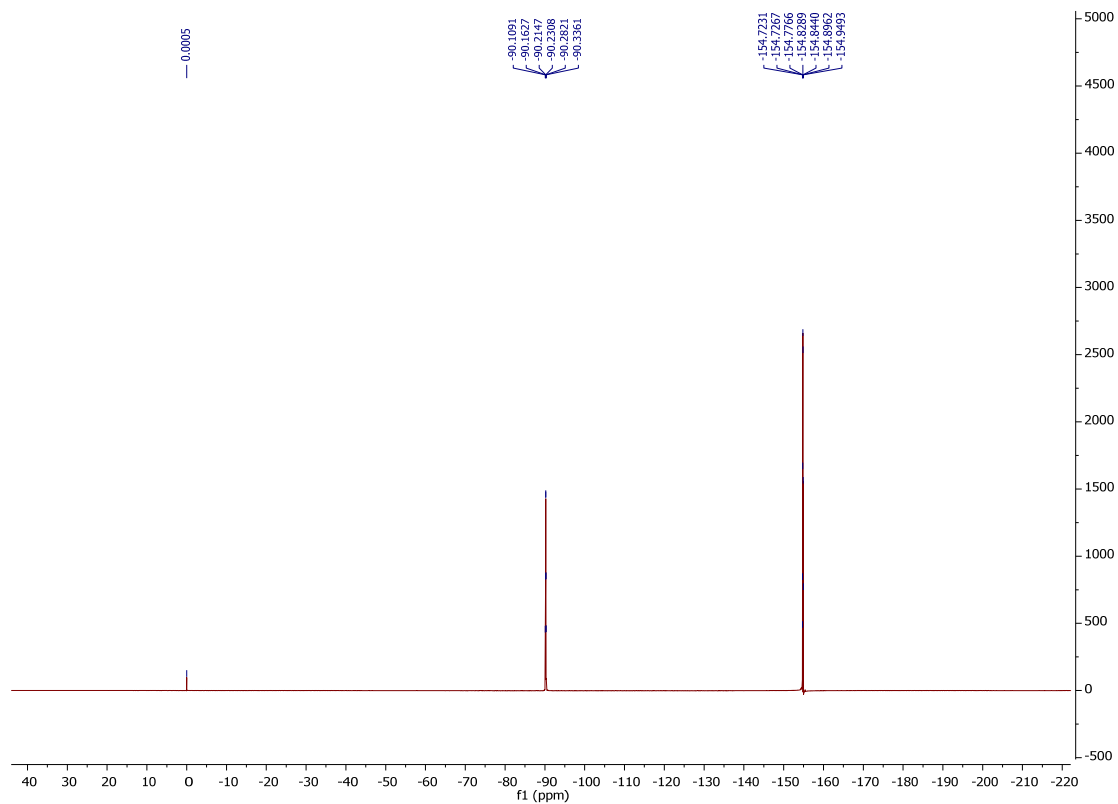


Figure S2. ^{19}F NMR spectrum of **1**

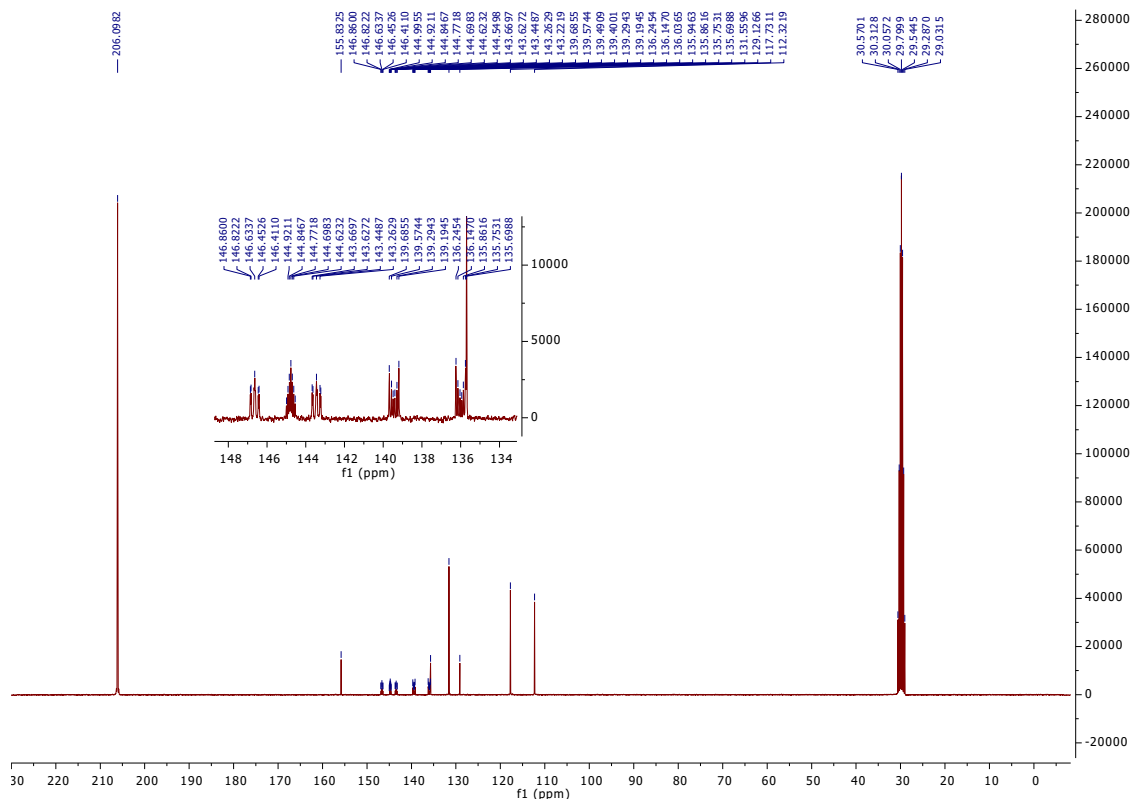


Figure S3. ¹³C NMR spectrum of **1**

Single Mass Analysis

Tolerance = 5.0 PPM / DBE: min = -1.5, max = 150.0

Element prediction: Off

Number of isotope peaks used for i-FIT = 3

Monoisotopic Mass, Even Electron Ions

382 formula(e) evaluated with 4 results within limits (all results (up to 1000) for each mass)

Elements Used:

C: 0-150 H: 0-150 N: 0-10 O: 0-15 F: 8-8

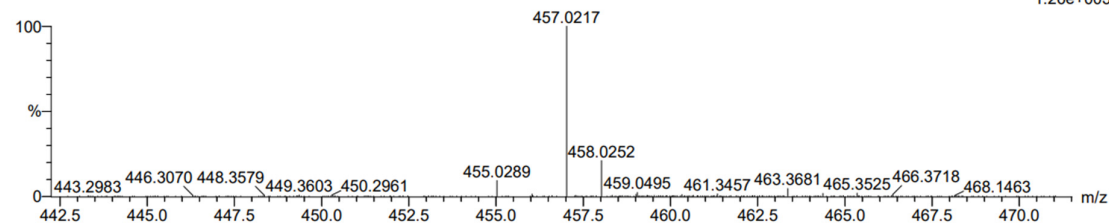
Olfa ZAYENE

Infusion - 10-4 M_ 0.5 KV 10V - 5ul/min

ZO96-10-4-(01) 13 (0.503) Cm (10:15)

21-Mar-2024

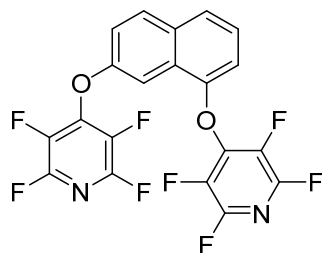
1: TOF MS ES-
1.26e+003



Minimum: -1.5
Maximum: 5.0 5.0 150.0

Mass	Calc. Mass	mDa	PPM	DBE	i-FIT	i-FIT (Norm)	Formula
457.0217	457.0215	0.2	0.4	3.5	104.5	5.5	C4 H5 N10 O7 F8
	457.0223	-0.6	-1.3	15.5	99.9	0.9	C20 H5 N2 O2 F8
	457.0202	1.5	3.3	-1.5	106.1	7.0	C3 H9 N6 O11 F8
	457.0196	2.1	4.6	16.5	99.6	0.6	C16 H N8 F8

Figure S4. High resolution mass spectrum of **1**



2

Purification conditions: Petroleum ether/Ethyl acetate 90/10

Aspect: Yellow solid

Yield: 39%

¹H NMR (300 MHz, Acetone δ 6, TMS): δ (ppm) 8.19 (d, 1H, $^3J_{\text{H-H}} = 9$ Hz), 8.10 (d, 1H, $^4J_{\text{H-H}} = 2.5$ Hz), 7.90 (d, 1H, $^3J_{\text{H-H}} = 8$ Hz), 7.68 (dd, 1H, $^3J_{\text{H-H}} = 8.3$ Hz, $^4J_{\text{H-H}} = 2.5$ Hz), 7.49 (t, 1H, $^3J_{\text{H-H}} = 8.3$ Hz), 7.35 (d, 1H, $^3J_{\text{H-H}} = 7.9$ Hz)

¹⁹F NMR (282 MHz, Acetone δ 6, CFCl_3): δ (ppm) -90.45 (m, 4F), -155.05 (m, 2F), -155.4 (m, 2F)

¹³C NMR (75 MHz, Acetone δ 6, TMS): δ (ppm): 155.4, 152.5, 146.8-143.3 (large d, m, 2C $^1J_{\text{C-F}} = 240.3$ Hz), 145.4-144.8 (m, 2C), 139.5-135.5 (large d, m $^1J_{\text{C-F}} = 259$ Hz) 133.2, 131.8, 126.3, 125.9, 119.4, 112.8, 107.2.

Rf: 0.6

HRMS (ESI(-)/Q-TOF) m/z [M-H]⁻: calculated for: 457.0223 found 457.0213

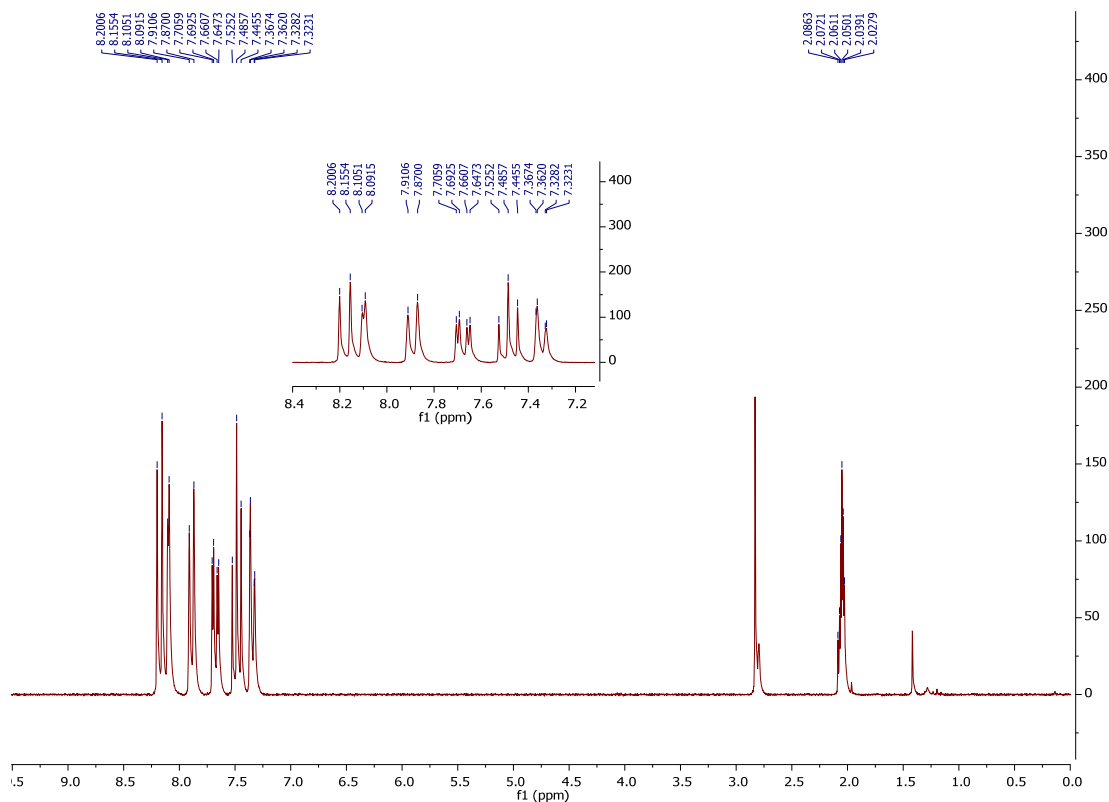


Figure S5. ¹H NMR spectrum of 2

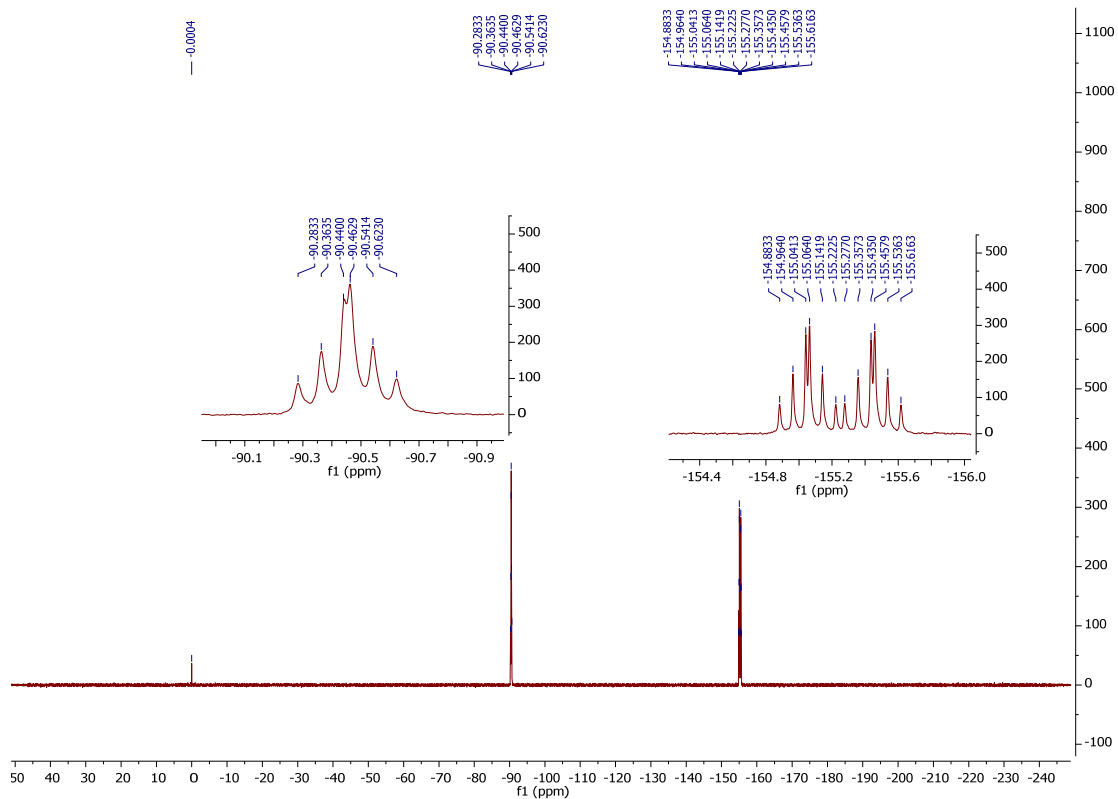


Figure S6. ^{19}F NMR spectrum of **2**

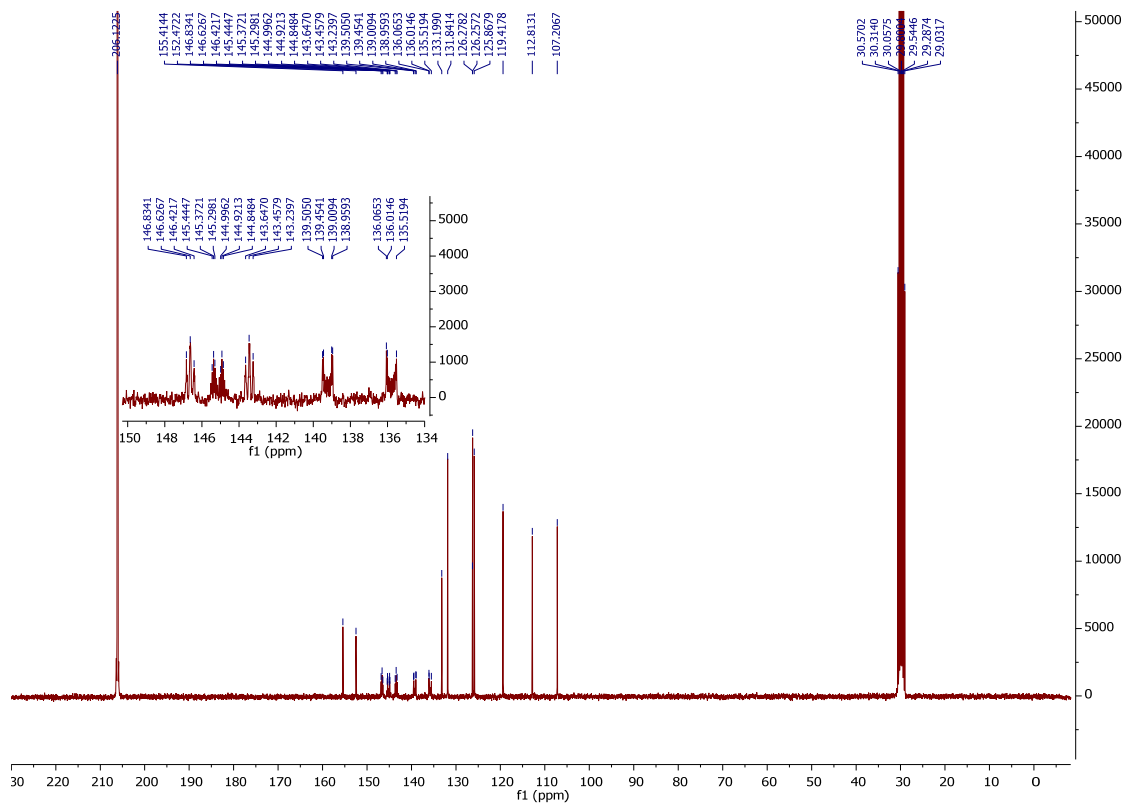


Figure S7. ^{13}C NMR spectrum of **2**

Single Mass Analysis

Tolerance = 5.0 PPM / DBE: min = -1.5, max = 150.0

Element prediction: Off

Number of isotope peaks used for i-FIT = 3

Monoisotopic Mass, Even Electron Ions

382 formula(e) evaluated with 4 results within limits (all results (up to 1000) for each mass)

Elements Used:

C: 0-150 H: 0-150 N: 0-10 O: 0-15 F: 8-8

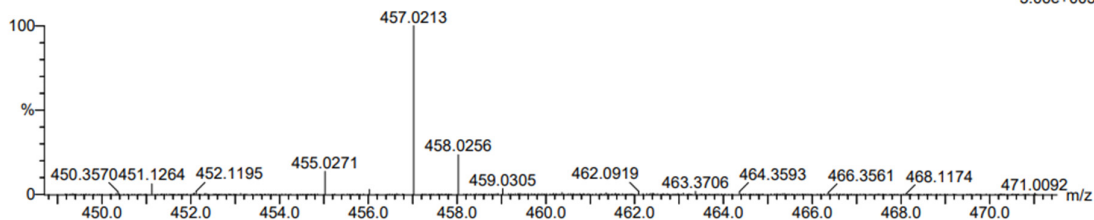
Olfa ZAYENE

Infusion - 10-4 M 0.7 KV 12V

ZO195-10-4-(01) 23 (0.884) Cm (19:25)

21-Feb-2024

1: TOF MS ES-
5.06e+003



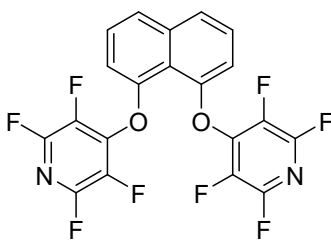
Minimum:

Maximum: 5.0 5.0 -1.5

Mass	Calc. Mass	mDa	PPM	DBE	i-FIT	i-FIT (Norm)	Formula
457.0213	457.0223	-1.0	-2.2	15.5	162.2	0.0	C20 H5 N2 O2 F8
	457.0196	1.7	3.7	16.5	169.2	7.0	C16 H N8 F8
	457.0215	-0.2	-0.4	3.5	175.2	13.0	C4 H5 N10 O7 F8
	457.0202	1.1	2.4	-1.5	175.8	13.6	C3 H9 N6 O11 F8

Figure S8. High resolution mass spectrum of 2

Procedure for 3: naphthalene-diol derivative (100mg, 0.6mmol) and K_2CO_3 were added to a round bottom flask. Pentafluoropyridine (211mg, 2eq) and 3 mL of acetonitrile were added under argon atmosphere. The mixture was stirred at room temperature overnight. The intermediate resulting from monosubstitution was obtained with traces of 3. 2 more equivalents of pentafluoropyridine and k_2CO_3 were added to the mixture. The mixture was stirred overnight. The mixture was diluted with OEtAc (15mL) and washed with water (3x10mL) and Brine (20mL). The Crude was dried over $MgSO_4$ and vaccued. The crude was purified over column chromatography.



3

Purification conditions: Petroleum ether/Toluene 80/20

Yield: 80%

Aspect: white solid

1H NMR (300 MHz, Acetone $\delta 6$, TMS): δ (ppm) 8.00 (dd, 2H, $^3J_{H-H}$ = 8.3 Hz), 7.66 (t, 2H, $^3J_{H-H}$ = 7.6 Hz), 7.53 (d, 2H, $^3J_{H-H}$ = 7.5 Hz).

^{19}F NMR (282 MHz, Acetone $\delta 6$, $CFCl_3$): δ (ppm) -90.87 (m, 4F), -157.24 (m, 4F).

^{13}C NMR (75 MHz, Acetone $\delta 6$, TMS): δ (ppm): 151.4 146.8-143.2 (large d, m, 2C, $^1J_{C-F}$ = 240Hz), 145.8 (m, 2C), 138.6-134.6 (large d, m, 2C, $^1J_{C-F}$ =258 Hz), 138.1, 127.9, 127.1, 118.3, 116.2

HRMS (ESI(-)/Q-TOF) m/z [M-H]⁻: calculated for: 457.0223 found: 457.0219.

Rf: 0.3

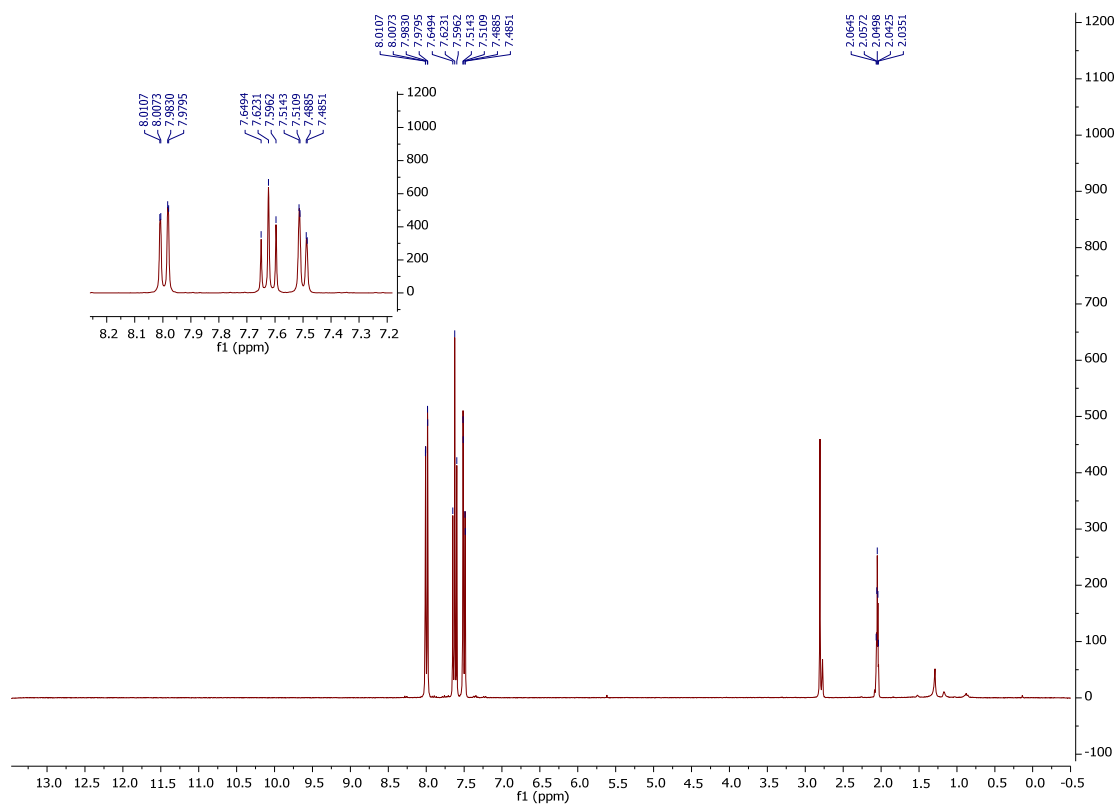


Figure S9. ¹H NMR spectrum of **3**

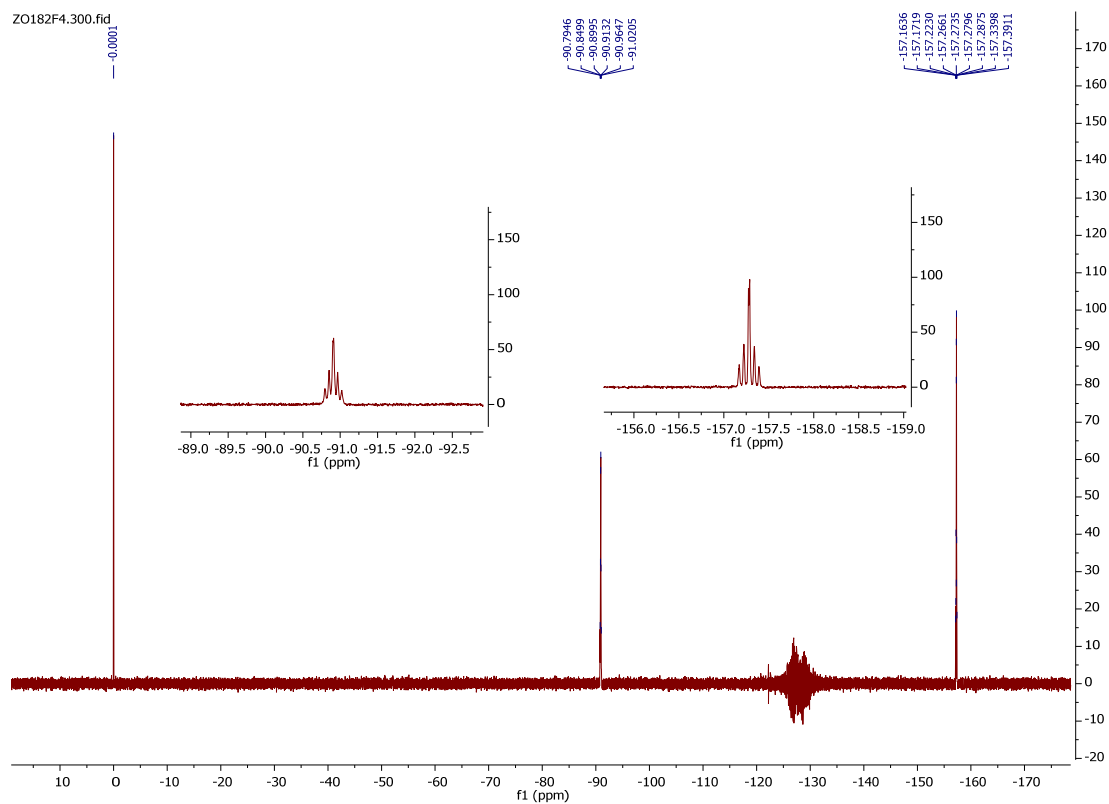


figure S10 ¹⁹F NMR spectrum of **3**

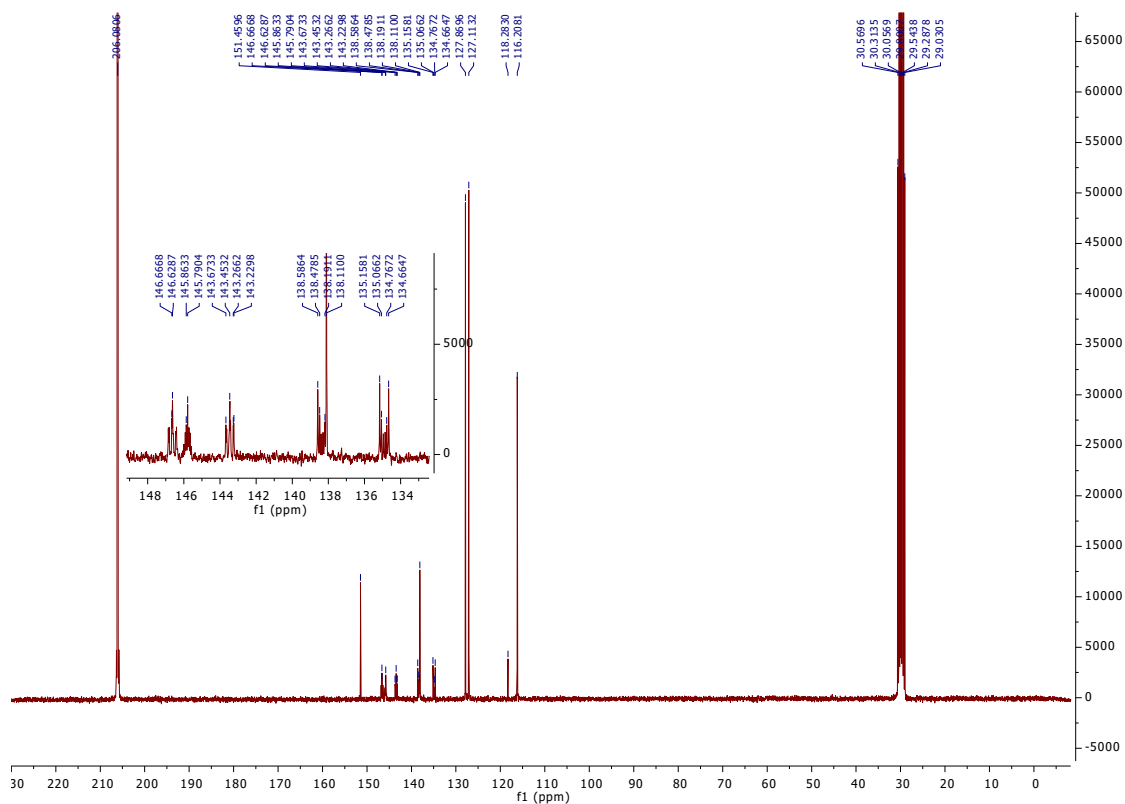


Figure S11. ¹³C NMR spectrum of **3**

Single Mass Analysis

Tolerance = 5.0 PPM / DBE: min = -1.5, max = 150.0

Element prediction: Off

Number of isotope peaks used for i-FIT = 3

Monoisotopic Mass, Even Electron Ions

382 formula(e) evaluated with 5 results within limits (all results (up to 1000) for each mass)

Elements Used:

C: 0-150 H: 0-150 N: 0-10 O: 0-15 F: 8-8

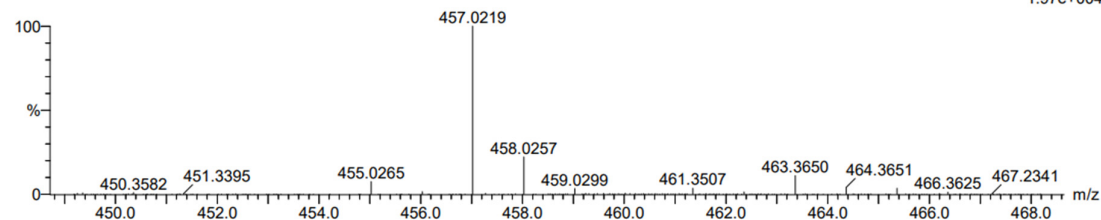
Olfa ZAYENE

Infusion - 10-4 M _ 1.5 KV 10V

ZO182-10-4-(01) 8 (0.312) Cm (8:13)

21-Mar-2024

1: TOF MS ES-
1.97e+004



Minimum:

Maximum: 5.0 5.0 -1.5 150.0

Mass	Calc. Mass	mDa	PPM	DBE	i-FIT	i-FIT (Norm)	Formula
457.0219	457.0223	-0.4	-0.9	15.5	146.0	0.0	C20 H5 N2 O2 F8
	457.0215	0.4	0.9	3.5	160.4	14.4	C4 H5 N10 O7 F8
	457.0202	1.7	3.7	-1.5	161.0	15.0	C3 H9 N6 O11 F8
	457.0242	-2.3	-5.0	2.5	157.8	11.8	C8 H9 N4 O9 F8
	457.0196	2.3	5.0	16.5	153.9	7.9	C16 H N8 F8

Figure S12. High resolution mass spectrum of **3**

3. Mass spectrometry analysis:

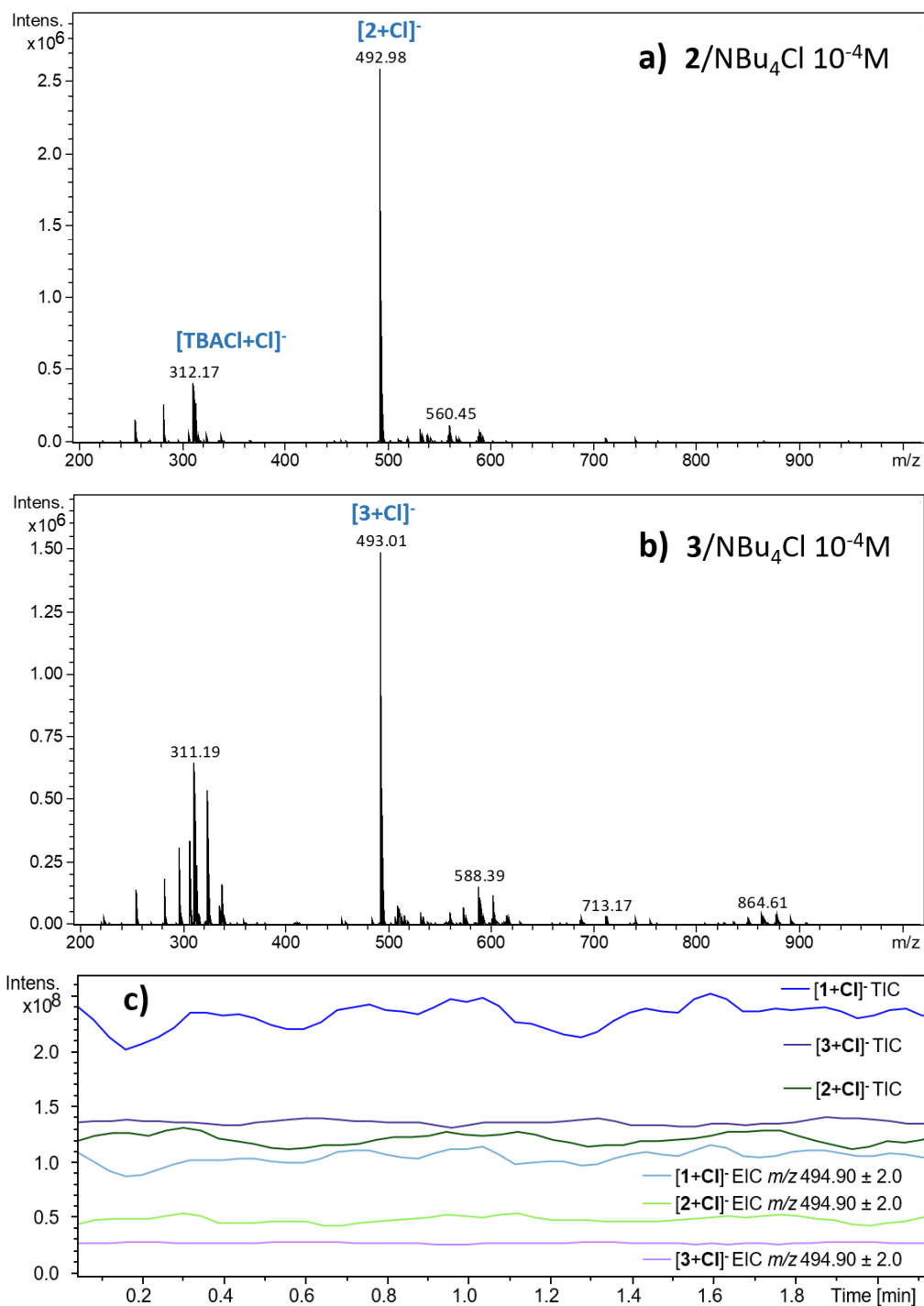


Figure S13. Electrospray mass spectrum of an equimolar (10⁻⁴ M) mixture of **a)** 2/NBu₄Cl **b)** 3/NBu₄. **c)** Total ion current (TIC) and extracted ion chromatogram (EIC) of [n+Cl]⁻ ion for the different mixtures. Experiments performed on the AMAZON SPEED ETD ion trap.

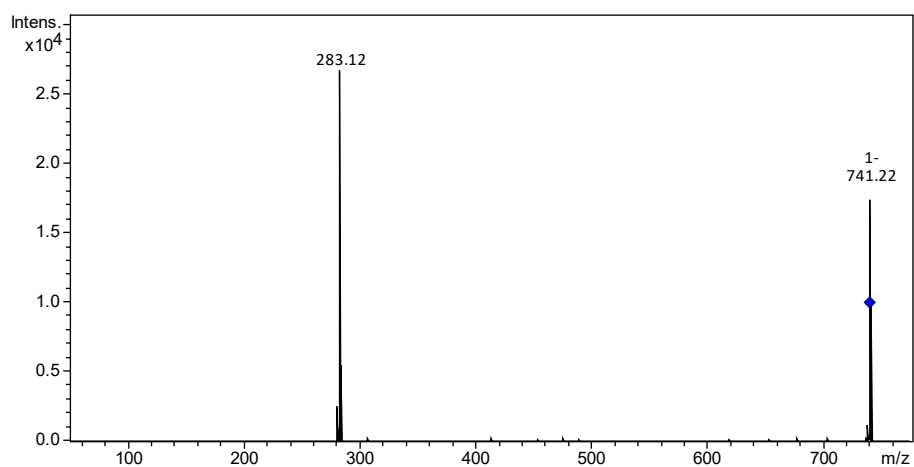


figure S14. CID mass spectrum of the m/z 741 ion recorded on the AMAZON SPEED ETD ion trap.

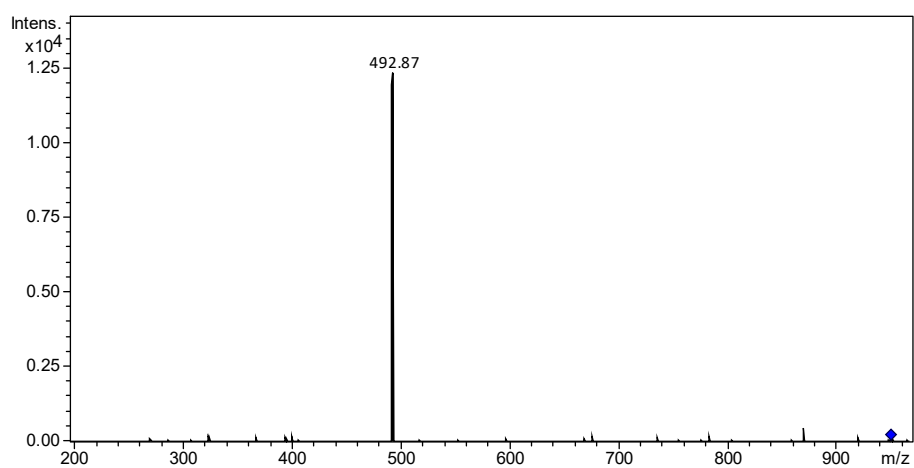


figure S15. CID mass spectrum of the ion [(1)₂+Cl]⁻ (m/z 951) recorded on the AMAZON SPEED ETD ion trap

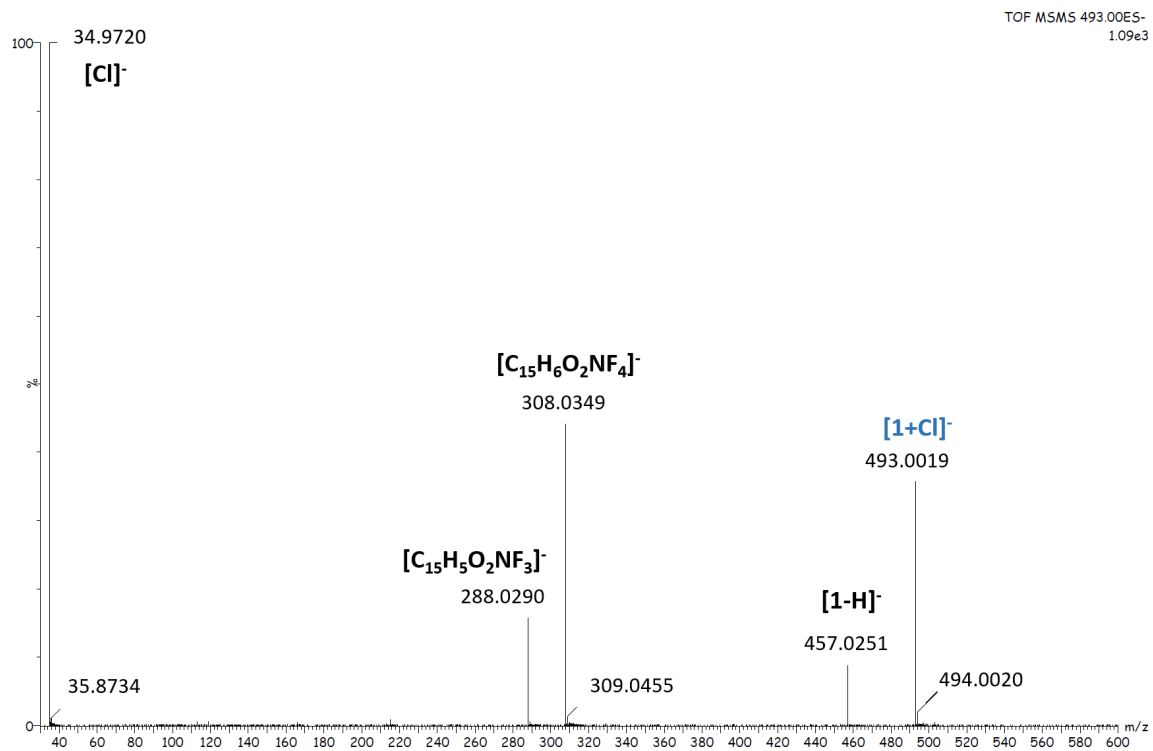


figure S16. CID mass spectrum of the ion [1+Cl]⁻ (m/z 493), recorded with the XEVO QTOF instrument (waters) at a collision energy of 14 eV (laboratory frame). Mass selection : 493.0 ± 1.0. The peak involving the ³⁷Cl atom (m/z 495) is presently not selected.

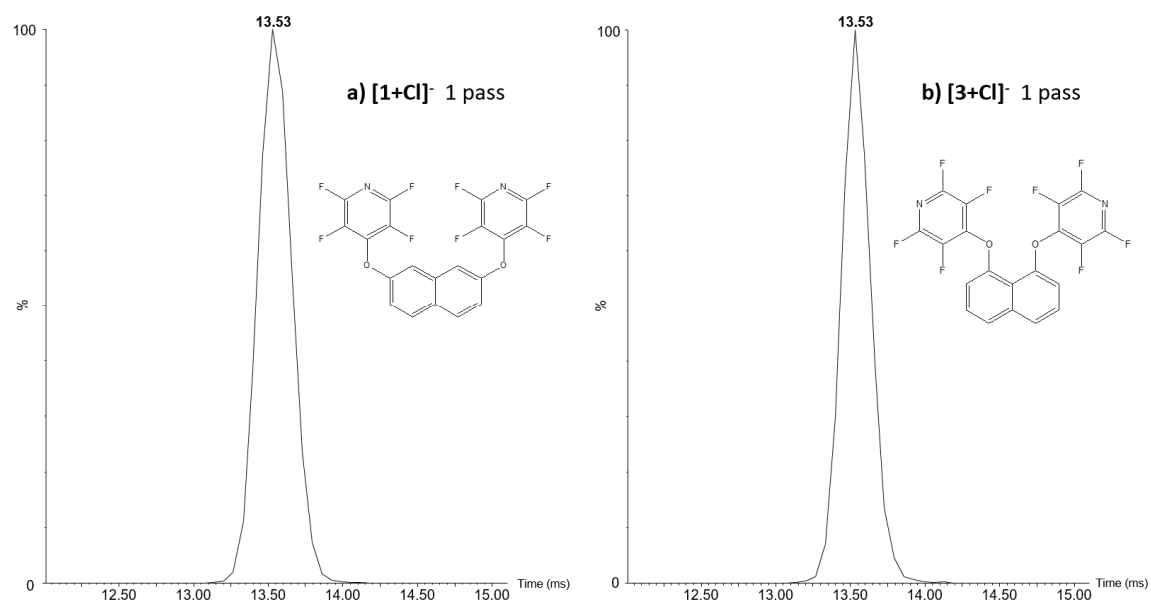


figure S17. Ion mobility mobilograms recorded for **a)** the ion [1+Cl]⁻ and **b)** the ion [3+Cl]⁻ after a single pass within the cyclic mobility cell

4. NMR titration

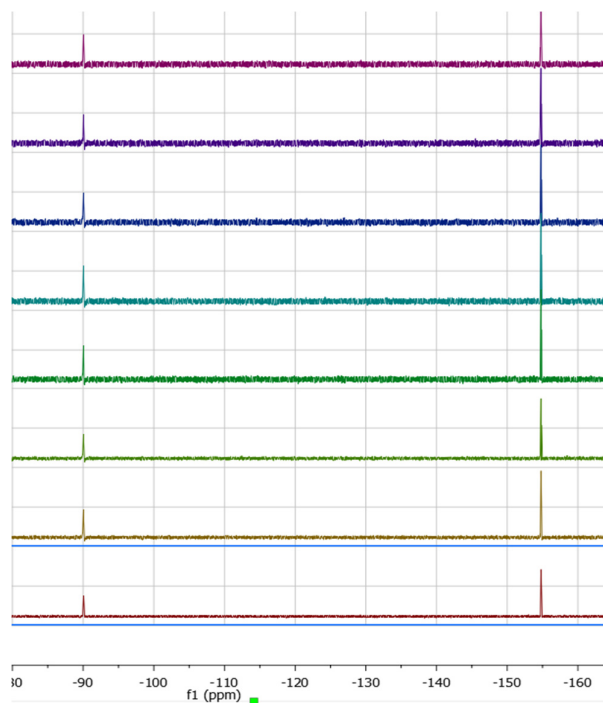


figure S18. NMR ¹⁹F titration in ACN-d₃ at 3.5 · 10⁻³ M of 1 with tetrabutylammonium chloride

5. DFT Analysis:

5.1 Interaction Energies calculation:

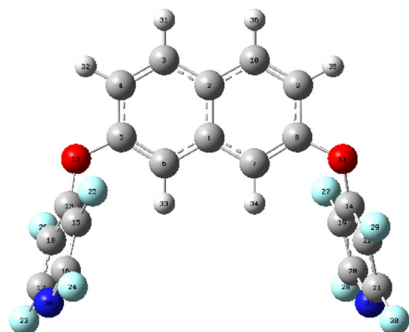
	E+ZPE(complex)	E+ZPE(ligand)	E (Cl ⁻)	E _{interaction}
[1a+Cl]⁻	-2283.226593	-1823.004878	-460.173093	-127.7
[2a+Cl]⁻	-2283.22319	-1823.005111	-460.173093	-118.1
[3b+Cl]⁻	-2283.221718	-1823.009656	-460.173093	-102.3
[4+Cl]⁻	-1489.699949	-1029.493465	-460.173093	-87.6
[5+Cl]⁻	-1489.699094	-1029.499625	-460.173093	-69.2
[6+Cl]⁻	-1489.697798	-1029.496898	-460.173093	-73.0

Energies expressed in Hartrees, Interaction energies in kJ/mol

$$\begin{aligned} E_{interaction,vacuum} &= \text{Energy of complexation vacuum} \\ &= E_{complex,vacuum} - E_{ligand,vacuum} - E_{ion,vacuum} \end{aligned}$$

ZPE taken into account

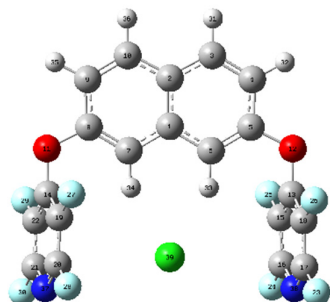
5.2 Coordinates and thermodynamics data of **1**



1 (in vacuum)
 APFD/Aug-cc-pVDZ
 Charge: 0
 Spin Multiplicity: Singlet
 Imaginary frequencies: 0
 Electronic Energy (RAPFD): -1823.234425 Hartree
 Zero-point energy correction= 0.229547 Hartree
 Thermal correction to Energy= 0.254582 Hartree
 Thermal correction to Enthalpy= 0.255526 Hartree
 Thermal correction to Gibbs Free Energy= 0.170392 Hartree
 Sum of electronic and zero-point Energies= -1823.004878 Hartree
 Sum of electronic and thermal Energies= -1822.979843 Hartree
 Sum of electronic and thermal Enthalpies= -1822.978899 Hartree
 Sum of electronic and thermal Free Energies= -1823.064033 Hartree

Center Number	Coordinates in Angstrom			Center Number	Coordinates in Angstrom		
	X	Y	Z		X	Y	Z
1	0.000004	1.885111	-0.000004	20	3.907348	-1.736211	-1.504762
2	0.000003	3.313451	0.000002	21	4.566382	-2.190792	0.599712
3	-1.23012	3.999905	-0.163765	22	4.304617	-0.895513	1.035782
4	-2.411133	3.314272	-0.313237	23	-5.035916	-3.078218	-1.476211
5	-2.390341	1.903514	-0.304468	24	-3.718539	-2.164744	2.753375
6	-1.224396	1.190241	-0.162062	25	-3.173683	0.432685	2.13815
7	1.224404	1.190241	0.162048	26	-4.512865	-0.534534	-2.302157
8	2.390348	1.903514	0.304461	27	3.173694	0.432676	-2.138158
9	2.411139	3.314272	0.31324	28	3.71854	-2.164759	-2.75337
10	1.230125	3.999905	0.163774	29	4.512856	-0.53453	2.302157
11	3.629219	1.308334	0.502857	30	5.035897	-3.078221	1.476224
12	-3.62921	1.308333	-0.502871	31	-1.230019	5.091048	-0.165635
13	-3.812633	0.028553	-0.111824	32	-3.363874	3.827878	-0.436388
14	3.812636	0.028551	0.111818	33	-1.229085	0.10028	-0.17217
15	-3.618227	-0.410819	1.204308	34	1.229094	0.100279	0.172148
16	-3.907349	-1.736201	1.504765	35	3.363879	3.827878	0.436396
17	-4.566394	-2.190787	-0.599704	36	1.230023	5.091048	0.165652
18	-4.304623	-0.895513	-1.035781	37	4.369258	-2.599585	-0.630716
19	3.618232	-0.410826	-1.204312	38	0.1725272	0.0737841	0.0632675

5.3 Coordinates and thermodynamics data of [1a+Cl]⁻



[1a+Cl]⁻ (in vacuum)

APFD/Aug-cc-pVDZ

Charge: -1

Spin Multiplicity: Singlet

Imaginary frequencies: 0

Electronic Energy (RAPFD): -2283.455504 Hartree

Zero-point energy correction= 0.228911 Hartree

Thermal correction to Energy= 0.256365 Hartree

Thermal correction to Enthalpy= 0.257309 Hartree

Thermal correction to Gibbs Free Energy= 0.165213 Hartree

Sum of electronic and zero-point Energies= -2283.226593 Hartree

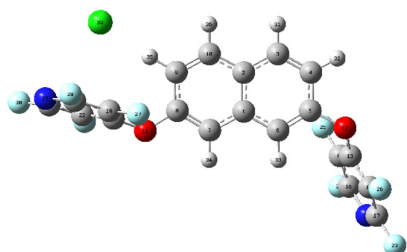
Sum of electronic and thermal Energies= -2283.199139 Hartree

Sum of electronic and thermal Enthalpies= -2283.198195 Hartree

Sum of electronic and thermal Free Energies= -2283.290292 Hartree

Center Number	Coordinates in A			Center Number	Coordinates in A		
	X	Y	Z		X	Y	Z
1	0.001789	2.17821	-0.001327	20	-3.316839	-1.903736	1.319131
2	0.002295	3.603743	0.000488	21	-3.987157	-1.98592	-0.823543
3	1.253795	4.273915	-0.035638	22	-3.964487	-0.603679	-0.958882
4	2.436339	3.567614	-0.070217	23	4.340517	-2.729904	1.882762
5	2.396821	2.153997	-0.060702	24	3.029511	-2.560731	-2.445088
6	1.218232	1.457163	-0.021297	25	2.927706	0.164233	-2.417586
7	-1.215169	1.458018	0.017058	26	4.270004	-0.014561	2.120512
8	-2.393247	2.155576	0.058985	27	-2.913794	0.167552	2.412763
9	-2.431738	3.569185	0.071883	28	-3.02059	-2.557039	2.443173
10	-1.248702	4.27473	0.038513	29	-4.284429	-0.012512	-2.116919
11	-3.635384	1.521967	0.071714	30	-4.359243	-2.727453	-1.876142
12	3.638366	1.519337	-0.074417	31	1.27305	5.366065	-0.036902
13	3.610218	0.161659	-0.150464	32	3.402236	4.072737	-0.099867
14	-3.609542	0.16446	0.149628	33	1.151075	0.359655	-0.002202
15	3.277002	-0.517923	-1.324127	34	-1.148837	0.360513	-0.004279
16	3.320341	-1.906962	-1.319788	35	-3.397261	4.07492	0.103235
17	3.976729	-1.988614	0.827187	36	-1.267168	5.366888	0.042448
18	3.956203	-0.606155	0.961066	37	-3.688465	-2.616709	0.283696
19	-3.270708	-0.514769	1.321941	38	3.683977	-2.61973	-0.281433
				39	0.00084	-1.693262	-0.001606

5.4 Coordinates and thermodynamics data of $[1b+Cl]^-$



$[1b+Cl]^-$ (in vacuum)

APFD/Aug-cc-pVDZ

Charge: -1

Spin Multiplicity: Singlet

Imaginary frequencies: 0

Electronic Energy (RAPFD): -2283.446713 Hartree

Zero-point energy correction= 0.229354 Hartree

Thermal correction to Energy= 0.256687 Hartree

Thermal correction to Enthalpy= 0.257631 Hartree

Thermal correction to Gibbs Free Energy= 0.166507 Hartree

Sum of electronic and zero-point Energies= -2283.217359 Hartree

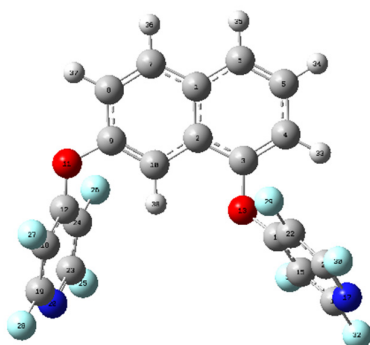
Sum of electronic and thermal Energies= -2283.190026 Hartree

Sum of electronic and thermal Enthalpies= -2283.189082 Hartree

Sum of electronic and thermal Free Energies= -2283.280206 Hartree

Center Number	Coordinates (in Angstroms)			Center Number	Coordinates (in Angstroms)		
	X	Y	Z		X	Y	Z
1	0.687931	0.724631	-0.102193	21	-5.994955	-1.552259	0.024993
2	0.213867	1.910803	-0.748091	22	-4.649117	-1.731012	-0.261983
3	1.140848	2.932894	-1.071189	23	7.418909	-1.390664	2.009898
4	2.480922	2.804931	-0.7811	24	5.570819	-2.469525	-1.976706
5	2.92243	1.628089	-0.147362	25	4.073374	-0.212002	-2.026222
6	2.069704	0.610494	0.20073	26	5.967089	0.903472	2.181008
7	-0.234618	-0.293614	0.231392	27	-3.359922	0.71965	2.066944
8	-1.565494	-0.12678	-0.077205	28	-6.049035	0.909449	2.448724
9	-2.061292	1.027501	-0.724905	29	-4.244707	-2.619067	-1.177345
10	-1.169252	2.023034	-1.043305	30	-6.892777	-2.306443	-0.622431
11	-2.394492	-1.192708	0.228816	31	0.773617	3.834908	-1.563896
12	4.290986	1.592291	0.170629	32	3.203046	3.582423	-1.028311
13	4.94157	0.422818	0.097986	33	2.441187	-0.282229	0.706189
14	-3.717554	-0.961684	0.430443	34	0.098513	-1.204234	0.729738
15	4.862674	-0.470571	-0.982666	35	-3.135703	1.133987	-0.986314
16	5.64559	-1.617282	-0.949842	36	-1.539344	2.919093	-1.545305
17	6.56829	-1.079524	1.02525	37	-6.449061	-0.706998	0.915875
18	5.833944	0.094421	1.125716	38	6.477664	-1.918582	0.020664
19	-4.205756	-0.044685	1.36257	39	-5.218608	1.488986	-1.594792
20	-5.578214	0.043102	1.542965				

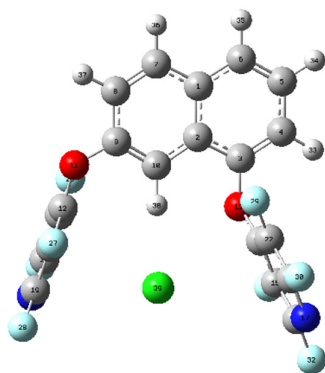
5.5 Coordinates and thermodynamics data of 2



2 (in vacuum)
 APFD/Aug-cc-pVDZ
 Charge: 0
 Spin Multiplicity: Singlet
 Imaginary frequencies: 0
 Electronic Energy (RAPFD): -1823.234706 Hartree
 Zero-point energy correction= 0.229595 Hartree
 Thermal correction to Energy= 0.254678 Hartree
 Thermal correction to Enthalpy= 0.255622 Hartree
 Thermal correction to Gibbs Free Energy= 0.170189 Hartree
 Sum of electronic and zero-point Energies= -1823.005111 Hartree
 Sum of electronic and thermal Energies= -1822.980029 Hartree
 Sum of electronic and thermal Enthalpies= -1822.979084 Hartree
 Sum of electronic and thermal Free Energies= -1823.064517 Hartree

Center Number	Coordinates in Angstrom			Center Number	Coordinates in Angstrom		
	X	Y	Z		X	Y	Z
1	0.128207	3.521793	-0.235938	20	-3.850682	-2.68421	-0.316599
2	0.196528	2.09636	-0.238623	21	4.279598	-1.128589	1.383667
3	1.448519	1.498614	-0.524403	22	3.186526	-0.335694	1.057658
4	2.570564	2.244633	-0.796608	23	-3.563967	-1.817898	-1.260153
5	2.487547	3.655127	-0.779357	24	-3.355787	-0.463795	-1.028165
6	1.293234	4.282364	-0.507493	25	-3.481168	-2.273366	-2.510239
7	-1.12143	4.13259	0.05065	26	-3.088163	0.380463	-2.02598
8	-2.238805	3.378929	0.313092	27	-3.837503	-0.536786	2.56011
9	-2.140261	1.970845	0.303194	28	-4.233262	-3.142396	1.864415
10	-0.956251	1.325079	0.044824	29	2.736858	0.604673	1.89208
11	-3.317553	1.308362	0.621321	30	4.893473	-0.92167	2.549377
12	-3.439277	0.003391	0.289686	31	2.481154	-1.837327	-2.161039
13	1.446454	0.10746	-0.5723	32	4.625206	-3.282948	-1.299148
14	2.551331	-0.555337	-0.172008	33	3.515226	1.750336	-1.024909
15	3.048991	-1.578385	-0.982356	34	3.382306	4.24084	-0.991777
16	4.143632	-2.307325	-0.529147	35	1.228218	5.371066	-0.497765
17	4.744209	-2.086374	0.615807	36	-1.185731	5.221515	0.056046
18	-3.743994	-0.923752	1.287712	37	-3.202553	3.838358	0.530328
19	-3.942189	-2.250569	0.917505	38	-0.889025	0.239331	0.052845

5.6 Coordinates and thermodynamics data of [2a+Cl]⁻



[2a+Cl]⁻(in vacuum)

APFD/Aug-cc-pVDZ

Charge: -1

Spin Multiplicity: Singlet

Imaginary frequencies: 0

Electronic Energy (RAPFD): -2283.452610 Hartree

Zero-point energy correction= 0.229421 Hartree

Thermal correction to Energy= 0.256671

Thermal correction to Enthalpy= 0.257615

Thermal correction to Gibbs Free Energy= 0.168290

Sum of electronic and zero-point Energies= -2283.223190

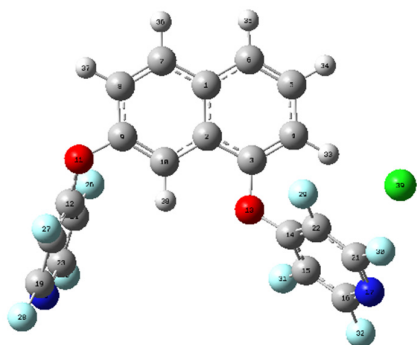
Sum of electronic and thermal Energies= -2283.195939

Sum of electronic and thermal Enthalpies= -2283.194995

Sum of electronic and thermal Free Energies= -2283.284320

Center Number	Coordinates in Angstrom			Center Number	Coordinates in Angstrom		
	X	Y	Z		X	Y	Z
1	0.69301	3.720546	0.030112	20	-3.921708	-2.067811	-0.688162
2	0.670089	2.311881	-0.213636	21	3.257444	-1.587222	1.571419
3	1.848141	1.728089	-0.751273	22	2.642481	-0.500329	0.969397
4	2.983329	2.459744	-1.000823	23	-3.570711	-1.069487	-1.459672
5	2.997792	3.846664	-0.726433	24	-3.149294	0.165299	-0.990108
6	1.871448	4.465194	-0.232915	25	-3.676842	-1.24662	-2.783316
7	-0.478178	4.330309	0.549653	26	-2.853023	1.164605	-1.832397
8	-1.599687	3.583421	0.815624	27	-3.319854	-0.611283	2.538098
9	-1.576346	2.189045	0.590775	28	-4.167204	-2.930161	1.389372
10	-0.472426	1.534372	0.098694	29	2.252894	0.551091	1.704618
11	-2.740722	1.537316	0.969114	30	3.481501	-1.536428	2.89508
12	-3.055924	0.351304	0.390968	31	2.634145	-1.815065	-2.397074
13	1.805986	0.398311	-1.144142	32	3.81716	-3.825825	-0.997957
14	2.406613	-0.550052	-0.40845	33	3.855209	1.960428	-1.423979
15	2.820426	-1.705546	-1.079018	34	3.90295	4.423039	-0.92443
16	3.41786	-2.719166	-0.351981	35	1.870425	5.538725	-0.034061
17	3.645175	-2.668824	0.941202	36	-0.477242	5.406126	0.734687
18	-3.39771	-0.723516	1.207597	37	-2.509017	4.037226	1.210411
19	-3.817702	-1.901721	0.606465	38	-0.457162	0.430635	0.02234
				39	-0.425557	-1.850032	-0.135425

5.7 Coordinates and thermodynamics data of $[2b+Cl]^-$



$[2b+Cl]^-$ (in vacuum)

APFD/Aug-cc-pVDZ

Charge: -1

Spin Multiplicity: Singlet

Imaginary frequencies: 0

Electronic Energy (RAPFD): -2283.446604 Hartree

Zero-point energy correction= 0.229469 Hartree

Thermal correction to Energy= 0.256843 Hartree

Thermal correction to Enthalpy= 0.257787 Hartree

Thermal correction to Gibbs Free Energy= 0.166329 Hartree

Sum of electronic and zero-point Energies= -2283.217135 Hartree

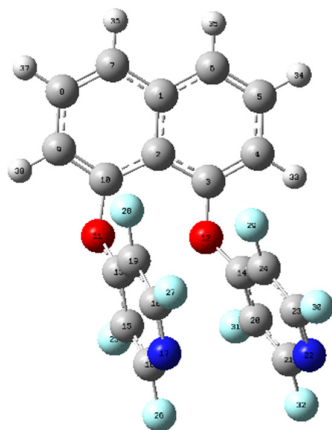
Sum of electronic and thermal Energies= -2283.189761 Hartree

Sum of electronic and thermal Enthalpies= -2283.188817 Hartree

Sum of electronic and thermal Free Energies= -2283.280275 Hartree

Center Number	Coordinates (in Angstroms)			Center Number	Coordinates (in Angstroms)		
	X	Y	Z		X	Y	Z
1	-0.108669	3.406806	-0.135408	21	4.047615	-1.374667	1.535341
2	-0.081678	1.981135	-0.036125	22	2.951952	-0.55823	1.297561
3	1.159377	1.324178	-0.240221	23	-4.135098	-1.522959	-1.434485
4	2.317847	2.006428	-0.524612	24	-3.77191	-0.2375	-1.053981
5	2.266239	3.416574	-0.607329	25	-4.024514	-1.862482	-2.721489
6	1.089778	4.108197	-0.423065	26	-3.342926	0.648333	-1.954356
7	-1.345424	4.071871	0.067936	27	-4.548678	-0.58318	2.466575
8	-2.498985	3.375885	0.348294	28	-5.219672	-3.030224	1.483103
9	-2.4379	1.972214	0.440329	29	2.577755	0.381547	2.175501
10	-1.27018	1.27296	0.268286	30	4.730885	-1.211648	2.675092
11	-3.642368	1.341956	0.787978	31	2.023569	-1.962757	-1.903874
12	-3.893943	0.117486	0.298425	32	4.179812	-3.475304	-1.205288
13	1.095539	-0.060889	-0.175915	33	3.284029	1.485364	-0.692676
14	2.230666	-0.746758	0.117637	34	3.194561	3.944792	-0.83115
15	2.665909	-1.743668	-0.750833	35	1.060864	5.197098	-0.494609
16	3.771975	-2.498565	-0.384895	36	-1.3724	5.16051	-0.006453
17	4.431482	-2.336784	0.734131	37	-3.453127	3.879599	0.500955
18	-4.397788	-0.856739	1.167228	38	-1.239259	0.188525	0.360712
19	-4.735648	-2.101034	0.651481	39	5.282153	0.626547	-1.019946
20	-4.606843	-2.431214	-0.611411				

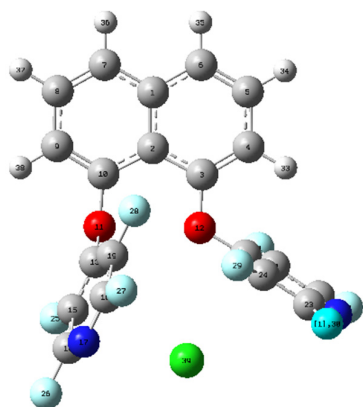
5.8 Coordinates and thermodynamics data of **3**



3 (in vacuum)
 APFD/Aug-cc-pVDZ
 Charge: 0
 Spin Multiplicity: Singlet
 Imaginary frequencies: 0
 Electronic Energy (RAPFD): -1823.239323 Hartree
 Zero-point energy correction= 0.229666 Hartree
 Thermal correction to Energy= 0.254458 Hartree
 Thermal correction to Enthalpy= 0.255402 Hartree
 Thermal correction to Gibbs Free Energy= 0.174255 Hartree
 Sum of electronic and zero-point Energies= -1823.009656 Hartree
 Sum of electronic and thermal Energies= -1822.984865 Hartree
 Sum of electronic and thermal Enthalpies= -1822.983920 Hartree
 Sum of electronic and thermal Free Energies= -1823.065068 Hartree

Center Number	Coordinates in Angstroms			Center Number	Coordinates in Angstroms		
	X	Y	Z		X	Y	Z
1	-3.815861	0.936834	-0.023841	20	2.036987	1.300927	-1.231173
2	-2.551126	0.431574	-0.476636	21	3.267891	1.440443	-0.604286
3	-1.473467	1.35746	-0.536381	22	3.425509	1.474191	0.698525
4	-1.613864	2.672491	-0.165278	23	2.356324	1.359911	1.447639
5	-2.853462	3.142471	0.312928	24	1.066926	1.205662	0.951581
6	-3.931707	2.292904	0.375292	25	1.079658	-1.80182	-2.408847
7	-4.946058	0.080279	0.012657	26	3.289452	-2.118504	-0.857903
8	-4.851098	-1.230521	-0.386772	27	0.838062	-2.011032	2.939626
9	-3.609254	-1.749241	-0.808937	28	-1.471383	-1.688454	1.595786
10	-2.496098	-0.948261	-0.830983	29	0.03113	1.053727	1.785774
11	-1.325994	-1.545046	-1.298912	30	2.523108	1.379844	2.769153
12	-0.266925	0.92605	-1.078255	31	1.931236	1.268433	-2.559836
13	-0.280553	-1.727119	-0.475597	32	4.359169	1.55439	-1.359127
14	0.890955	1.17533	-0.437918	33	-0.758856	3.343924	-0.248498
15	0.974025	-1.873996	-1.081599	34	-2.950806	4.185591	0.614671
16	2.091946	-2.031623	-0.277476	35	-4.89987	2.651009	0.726562
17	2.051401	-2.075656	1.034969	36	-5.896724	0.488373	0.3574
18	0.878029	-1.965645	1.608173	37	-5.72569	-1.881256	-0.367187
19	-0.320651	-1.796925	0.922673	38	-3.506255	-2.792393	-1.106104

5.9 Coordinates and thermodynamics data of $[3a+Cl]^-$



$[3a+Cl]^-$ (in vacuum)

APFD/Aug-cc-pVDZ

Charge: -1

Spin Multiplicity: Singlet

Imaginary frequencies: 0

Electronic Energy (RAPFD): -2283.439320 Hartree

Zero-point energy correction= 0.229205 Hartree

Thermal correction to Energy= 0.256676 Hartree

Thermal correction to Enthalpy= 0.257620 Hartree

Thermal correction to Gibbs Free Energy= 0.167449 Hartree

Sum of electronic and zero-point Energies= -2283.210115 Hartree

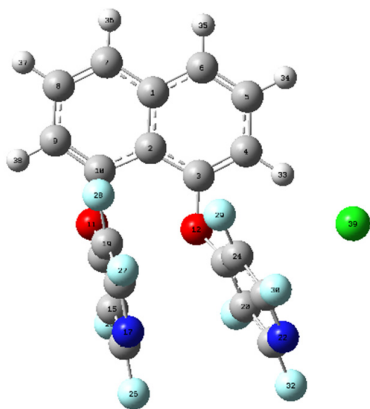
Sum of electronic and thermal Energies= -2283.182644 Hartree

Sum of electronic and thermal Enthalpies= -2283.181700 Hartree

Sum of electronic and thermal Free Energies= -2283.271871 Hartree

Center Number	Coordinates in Angstrom			Center Number	Coordinates in Angstrom		
	X	Y	Z		X	Y	Z
1	-2.680549	2.993901	0.146669	21	3.821727	1.230596	-0.864514
2	-1.878408	1.86196	-0.206898	22	4.341559	0.777166	0.250022
3	-0.465139	1.962384	-0.03253	23	3.522923	0.34771	1.180711
4	0.113924	3.1305	0.420716	24	2.140805	0.362809	1.063796
5	-0.691398	4.2451	0.734267	25	-1.428911	-2.715996	-2.395951
6	-2.057933	4.182532	0.609394	26	-0.737266	-4.912195	-0.947981
7	-4.093538	2.913404	0.041146	27	-0.895514	-2.602853	2.941944
8	-4.704563	1.762606	-0.396632	28	-1.59704	-0.314285	1.700211
9	-3.923968	0.648319	-0.769139	29	1.351519	-0.079539	2.041528
10	-2.55281	0.700467	-0.67999	30	4.07035	-0.117503	2.31148
11	-1.855994	-0.379762	-1.191272	31	1.97597	1.78565	-2.258292
12	0.247278	0.831708	-0.313851	32	4.671997	1.666339	-1.807609
13	-1.539493	-1.436761	-0.412265	33	1.194201	3.180218	0.546839
14	1.593001	0.84542	-0.120462	34	-0.212052	5.158338	1.090894
15	-1.297099	-2.642831	-1.070045	35	-2.683965	5.037537	0.867968
16	-0.937422	-3.750551	-0.31876	36	-4.686124	3.786548	0.319096
17	-0.819214	-3.746574	0.987757	37	-5.791778	1.707117	-0.471263
18	-1.022726	-2.610287	1.604349	38	-4.384318	-0.263475	-1.149037
19	-1.38932	-1.429167	0.977907	39	1.857448	-2.091466	-0.99345
20	2.458784	1.303951	-1.108937				

5.10 Coordinates and thermodynamics data of $[3b+Cl]^-$



$[3b+Cl]^-$ (in vacuum)

APFD/Aug-cc-pVDZ

Charge: -1

Spin Multiplicity: Singlet

Imaginary frequencies: 0

Electronic Energy (RAPFD): -2283.451089 Hartree

Zero-point energy correction= 0.229371Hartree

Thermal correction to Energy= 0.256530 Hartree

Thermal correction to Enthalpy= 0.257474 Hartree

Thermal correction to Gibbs Free Energy= 0.169598 Hartree

Sum of electronic and zero-point Energies= -2283.221718 Hartree

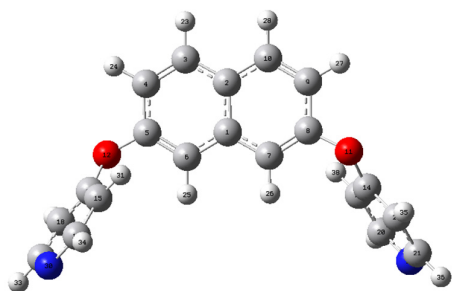
Sum of electronic and thermal Energies= -2283.194559 Hartree

Sum of electronic and thermal Enthalpies= -2283.193615 Hartree

Sum of electronic and thermal Free Energies= -2283.281492 Hartree

Center Number	Coordinates (in Angstroms)			Center Number	Coordinates (in Angstroms)		
	X	Y	Z		X	Y	Z
1	-3.718788	1.331904	-0.027061	21	3.351454	0.635777	-0.653623
2	-2.569623	0.58446	-0.456522	22	3.559658	0.659782	0.64043
3	-1.323251	1.271098	-0.478512	23	2.509929	0.712817	1.420434
4	-1.186151	2.579554	-0.08312	24	1.199422	0.709922	0.968018
5	-2.32341	3.278274	0.36873	25	0.529923	-2.367864	-2.392785
6	-3.56146	2.678339	0.387768	26	2.635899	-3.131492	-0.852674
7	-4.999741	0.721145	-0.027059	27	0.311176	-2.422951	2.962052
8	-5.166147	-0.581844	-0.430905	28	-1.89232	-1.64226	1.630019
9	-4.043942	-1.3403	-0.825828	29	0.175889	0.719458	1.835699
10	-2.792502	-0.77623	-0.818664	30	2.72339	0.73056	2.741528
11	-1.763048	-1.607664	-1.269394	31	1.944993	0.604973	-2.566214
12	-0.236098	0.582089	-0.999588	32	4.428237	0.586801	-1.448016
13	-0.761446	-1.961924	-0.451619	33	-0.191812	3.073808	-0.117441
14	0.976127	0.682842	-0.409795	34	-2.200417	4.31446	0.688043
15	0.429804	-2.377403	-1.061487	35	-4.445296	3.226991	0.718169
16	1.496051	-2.757449	-0.26365	36	-5.855657	1.315006	0.297835
17	1.463187	-2.774321	1.049615	37	-6.155587	-1.041302	-0.435322
18	0.348487	-2.398011	1.626613	38	-4.142987	-2.383338	-1.12557
19	-0.794973	-1.992476	0.948432	39	1.83027	3.939393	-0.108782
20	2.096114	0.638847	-1.239043				

5.11 Coordinates and thermodynamics data of 4



4 (in vacuum)
APFD/Aug-cc-pVDZ

Charge: 0

Spin Multiplicity: Singlet

Imaginary frequencies: 0

Electronic Energy (RAPFD): -1029.787072 Hartree

Zero-point energy correction= 0.293608 Hartree

Thermal correction to Energy= 0.311778 Hartree

Thermal correction to Enthalpy= 0.312722 Hartree

Thermal correction to Gibbs Free Energy= 0.242918 Hartree

Sum of electronic and zero-point Energies= -1029.493465 Hartree

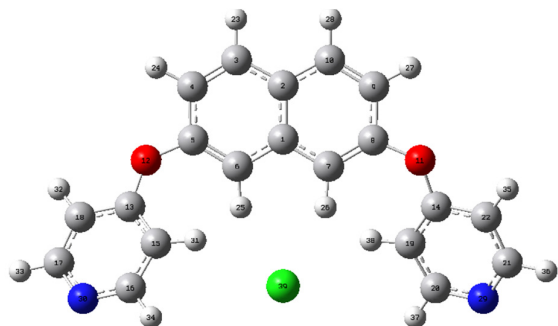
Sum of electronic and thermal Energies=-1029.475295 Hartree

Sum of electronic and thermal Enthalpies= -1029.474351 Hartree

Sum of electronic and thermal Free Energies= -1029.544154 Hartree

Center Number	Coordinates (in Angstroms)			Center Number	Coordinates (in Angstroms)		
	X	Y	Z		X	Y	Z
1	0.000018	1.127631	-0.000004	20	4.397516	-1.805811	-1.633189
2	0.000015	2.55812	-0.000008	21	5.430807	-2.431858	0.291589
3	-1.191669	3.243713	-0.347092	22	4.854622	-1.38936	1.012418
4	-2.337376	2.554744	-0.668891	23	-1.191064	4.334941	-0.350949
5	-2.325517	1.142043	-0.658087	24	-3.260425	3.069262	-0.934847
6	-1.186828	0.433985	-0.343621	25	-1.196791	-0.656	-0.35224
7	1.186866	0.433992	0.343618	26	1.196835	-0.655993	0.352241
8	2.325552	1.142057	0.658081	27	3.260455	3.069281	0.934824
9	2.337407	2.554758	0.668873	28	1.191088	4.334948	0.350918
10	1.191697	3.24372	0.34707	29	5.216677	-2.656222	-1.008991
11	3.495101	0.526311	1.058223	30	-5.216745	-2.656169	1.009008
12	-3.495065	0.526294	-1.058231	31	-3.106674	-0.068342	1.592772
13	-3.998954	-0.519711	-0.337778	32	-5.059639	-1.245861	-2.072763
14	3.998959	-0.519716	0.337783	33	-6.10334	-3.130852	-0.795284
15	-3.761649	-0.725502	1.023157	34	-4.234948	-1.991104	2.698105
16	-4.397602	-1.805747	1.633215	35	5.0597	-1.245831	2.072749
17	-5.430823	-2.431838	-0.291586	36	6.103337	-3.130865	0.79528
18	-4.854601	-1.389363	-1.01242	37	4.234819	-1.991196	-2.698068
19	3.761597	-0.725543	-1.023136	38	3.106602	-0.068394	-1.592742

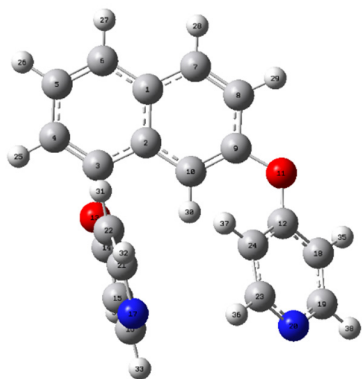
5.12 Coordinates and thermodynamics data of $[4+Cl]^-$



$[4+Cl]^-$ (in vacuum)
 APFD/Aug-cc-pVDZ
 Charge: -1
 Spin Multiplicity: Singlet
 Imaginary frequencies: 0
 Electronic Energy (RAPFD): -1489.994146 Hartree
 Zero-point energy correction=0.294197 Hartree
 Thermal correction to Energy= 0.314606 Hartree
 Thermal correction to Enthalpy= 0.315550 Hartree
 Thermal correction to Gibbs Free Energy= 0.240019 Hartree
 Sum of electronic and zero-point Energies= -1489.699949 Hartree
 Sum of electronic and thermal Energies= -1489.679540 Hartree
 Sum of electronic and thermal Enthalpies= -1489.678596 Hartree
 Sum of electronic and thermal Free Energies= -1489.754127 Hartree

Center Number	Coordinates (in Angstroms)			Center Number	Coordinates (in Angstroms)		
	X	Y	Z		X	Y	Z
1	0.000106	1.531811	0.000836	20	4.052613	-2.421137	-0.886027
2	0.00061	2.957406	-0.000383	21	5.960784	-1.750865	0.137584
3	-1.238526	3.63421	-0.133719	22	5.396481	-0.537518	0.503898
4	-2.41101	2.928809	-0.260108	23	-1.252971	4.726448	-0.130443
5	-2.391624	1.510044	-0.290376	24	-3.371848	3.435438	-0.357597
6	-1.210749	0.812276	-0.187428	25	-1.126497	-0.276775	-0.266792
7	1.210495	0.811839	0.190385	26	1.125733	-0.277024	0.27181
8	2.391835	1.509002	0.291975	27	3.373407	3.433819	0.355914
9	2.41222	2.927676	0.259341	28	1.255324	4.725854	0.126689
10	1.240177	3.633633	0.131808	29	5.315834	-2.700075	-0.552926
11	3.642595	0.96956	0.519539	30	-5.315888	-2.700478	0.548018
12	-3.642881	0.971432	-0.516908	31	-2.33556	-1.151272	0.889631
13	-4.073125	-0.263477	-0.131513	32	-5.959528	0.205002	-1.07256
14	4.072937	-0.26454	0.131721	33	-6.992704	-1.975546	-0.426076
15	-3.376335	-1.234952	0.589167	34	-3.510709	-3.200793	1.423106
16	-4.0537	-2.420907	0.884477	35	5.961317	0.204517	1.068507
17	-5.959872	-1.751136	-0.143211	36	6.994473	-1.974742	0.417731
18	-5.395556	-0.537079	-0.507152	37	3.508914	-3.200952	-1.424052
19	3.375048	-1.235985	-0.587961	38	2.333389	-1.152921	-0.885577
				39	-0.000996	-2.369398	0.003715

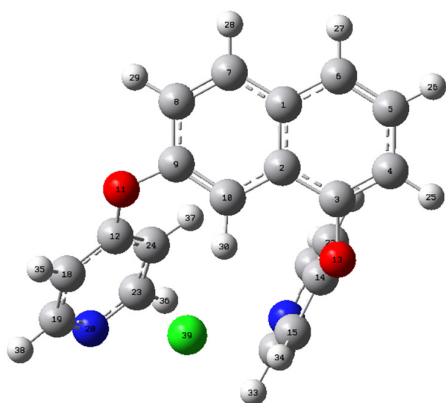
5.13 Coordinates and thermodynamics data of 5



5 (in vacuum)
 APFD/Aug-cc-pVDZ
 Charge: 0
 Spin Multiplicity: Singlet
 Imaginary frequencies: 0
 Electronic Energy (RAPFD): -1029.793820 Hartree
 Zero-point energy correction= 0.294195 Hartree
 Thermal correction to Energy= 0.312077 Hartree
 Thermal correction to Enthalpy= 0.313021 Hartree
 Thermal correction to Gibbs Free Energy= 0.246805 Hartree
 Sum of electronic and zero-point Energies= -1029.499625 Hartree
 Sum of electronic and thermal Energies= -1029.481743 Hartree
 Sum of electronic and thermal Enthalpies= -1029.480799 Hartree
 Sum of electronic and thermal Free Energies= -1029.547015 Hartree

Center Number	Coordinates (in Angstroms)			Center Number	Coordinates (in Angstroms)		
	X	Y	Z		X	Y	Z
1	-2.911734	1.322118	0.229455	20	4.45474	0.257921	-0.118797
2	-1.913747	0.468381	-0.327264	21	0.638838	-2.608245	1.665969
3	-2.30566	-0.835343	-0.741564	22	-0.447832	-2.11258	0.947365
4	-3.610347	-1.25534	-0.662566	23	3.410265	-0.086285	0.642096
5	-4.598144	-0.383758	-0.145063	24	2.228088	0.646751	0.731606
6	-4.255073	0.872401	0.302312	25	-3.865986	-2.261575	-0.994338
7	-2.511054	2.602679	0.69611	26	-5.632808	-0.723946	-0.089501
8	-1.198599	3.005452	0.633241	27	-5.012332	1.537782	0.719735
9	-0.22754	2.146408	0.066528	28	-3.264614	3.266789	1.122387
10	-0.575661	0.912338	-0.433056	29	-0.882347	3.980128	1.004575
11	1.046489	2.658155	0.001972	30	0.174985	0.275106	-0.892273
12	2.127814	1.812034	-0.031224	31	-1.319207	-1.705584	1.457609
13	-1.354826	-1.690086	-1.279034	32	0.610535	-2.593374	2.758577
14	-0.372804	-2.148852	-0.44683	33	2.698033	-3.552357	-0.664126
15	0.766493	-2.68289	-1.047689	34	0.850455	-2.719989	-2.133102
16	1.786947	-3.143562	-0.221402	35	3.151323	3.105392	-1.423408
17	1.74609	-3.112341	1.115503	36	3.512492	-1.0086	1.217255
18	3.204174	2.196162	-0.825646	37	1.412346	0.30675	1.366811
19	4.337213	1.384148	-0.827074	38	5.198178	1.657764	-1.442461

5.14 Coordinates and thermodynamics data of $[5+Cl]^-$



$[5+Cl]^-$ (in vacuum)

APFD/Aug-cc-pVDZ

Charge: -1

Spin Multiplicity: Singlet

Imaginary frequencies: 0

Electronic Energy (RAPFD): -1489.992800 Hartree

Zero-point energy correction= 0.293706 Hartree

Thermal correction to Energy= 0.313929 Hartree

Thermal correction to Enthalpy= 0.314873 Hartree

Thermal correction to Gibbs Free Energy= 0.242406 Hartree

Sum of electronic and zero-point Energies= -1489.699094 Hartree

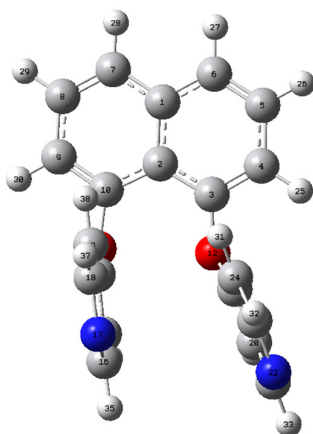
Sum of electronic and thermal Energies= -1489.678871 Hartree

Sum of electronic and thermal Enthalpies= -1489.677927 Hartree

Sum of electronic and thermal Free Energies= -1489.750394 Hartree

Center Number	X	Y	Z	Center Number	X	Y	Z
1	2.985349	-1.422548	0.394977	20	-4.348765	-0.078469	0.795032
2	2.030486	-0.536962	-0.19293	21	-0.137644	2.841481	1.836996
3	2.49348	0.732093	-0.651395	22	0.885972	2.300503	1.062051
4	3.82469	1.071528	-0.609953	23	-3.163258	0.236084	1.325709
5	4.767549	0.160036	-0.074959	24	-1.997159	-0.507446	1.156234
6	4.355376	-1.051039	0.434026	25	4.131702	2.051053	-0.976933
7	2.518363	-2.657654	0.914248	26	5.823129	0.436961	-0.048937
8	1.181605	-2.981756	0.865678	27	5.077173	-1.743766	0.871631
9	0.263929	-2.097972	0.252717	28	3.235292	-3.346947	1.364996
10	0.67097	-0.907121	-0.30588	29	0.80842	-3.920643	1.276635
11	-1.036313	-2.539403	0.190316	30	-0.048799	-0.317084	-0.892203
12	-2.070026	-1.657803	0.370641	31	1.840586	2.020355	1.506382
13	1.587679	1.632076	-1.168858	32	0.023149	2.999933	2.907508
14	0.642022	2.120871	-0.302335	33	-2.541187	3.228334	-0.315967
15	-0.600859	2.462862	-0.826978	34	-0.847754	2.221374	-1.862171
16	-1.543142	2.985862	0.054864	35	-3.354448	-2.861737	-0.870278
17	-1.336976	3.191022	1.363693	36	-3.127473	1.148814	1.924646
18	-3.287387	-1.998884	-0.210447	37	-1.062824	-0.175257	1.60438
19	-4.381569	-1.178776	0.034271	38	-5.345353	-1.416506	-0.424232
				39	-1.520873	-0.137311	-2.736083

5.15 Coordinates and thermodynamics data of 6



6 (in vacuum)

APFD/Aug-cc-pVDZ

Charge: 0

Spin Multiplicity: Singlet

Imaginary frequencies: 0

Electronic Energy (RAPFD): -1029.790714 Hartree

Zero-point energy correction= 0.293816 Hartree

Thermal correction to Energy= 0.311697 Hartree

Thermal correction to Enthalpy= 0.312641 Hartree

Thermal correction to Gibbs Free Energy= 0.246942 Hartree

Sum of electronic and zero-point Energies= -1029.496898 Hartree

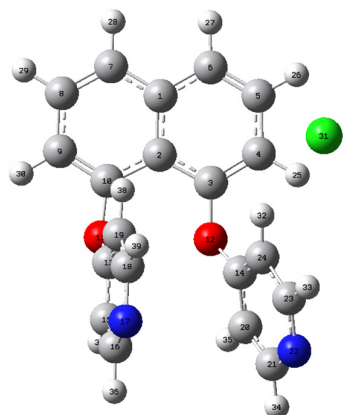
Sum of electronic and thermal Energies= -1029.479017 Hartree

Sum of electronic and thermal Enthalpies= -1029.478073 Hartree

Sum of electronic and thermal Free Energies= -1029.543772 Hartree

Center Number	Coordinates (in Angstroms)			Center Number	Coordinates (in Angstroms)		
	X	Y	Z		X	Y	Z
1	-3.164864	0.745308	0.264876	20	2.552845	1.257944	-1.496629
2	-1.92251	0.305164	-0.300718	21	3.846669	1.396226	-1.003897
3	-0.86125	1.254283	-0.382941	22	4.157172	1.422437	0.296176
4	-1.000975	2.529291	0.122126	23	3.140222	1.313096	1.154819
5	-2.211485	2.93002	0.722411	24	1.802802	1.182367	0.785766
6	-3.277089	2.062437	0.777686	25	-0.169228	3.22771	0.030953
7	-4.273595	-0.141078	0.304709	26	-2.302747	3.942925	1.116532
8	-4.170577	-1.421313	-0.182515	27	-4.227	2.37553	1.212505
9	-2.937883	-1.885209	-0.692615	28	-5.212362	0.218577	0.727883
10	-1.845598	-1.053095	-0.737162	29	-5.028468	-2.094245	-0.156364
11	-0.6694	-1.585651	-1.229873	30	-2.821574	-2.911876	-1.0392
12	0.268396	0.913642	-1.093355	31	1.021437	1.083399	1.535889
13	0.331649	-1.812458	-0.330661	32	3.405179	1.319401	2.214538
14	1.51223	1.142831	-0.576973	33	4.684209	1.489986	-1.699822
15	1.605081	-2.049689	-0.845028	34	2.34682	1.226294	-2.565705
16	2.644448	-2.263272	0.053957	35	3.65779	-2.427109	-0.319495
17	2.501216	-2.272967	1.384493	36	1.773517	-2.035519	-1.920653
18	1.26955	-2.061949	1.850284	37	1.158192	-2.079665	2.937688
19	0.150362	-1.823359	1.053353	38	-0.826636	-1.6509	1.501306

5.16 Coordinates and thermodynamics data of $[6+Cl]^-$



$[6+Cl]^-$ (in vacuum)

APFD/Aug-cc-pVDZ

Charge: -1

Spin Multiplicity: Singlet

Imaginary frequencies: 0

Electronic Energy (RAPFD): -1489.991716 Hartree

Zero-point energy correction= 0.293918 Hartree

Thermal correction to Energy= 0.314211 Hartree

Thermal correction to Enthalpy= 0.315156 Hartree

Thermal correction to Gibbs Free Energy= 0.241318 Hartree

Sum of electronic and zero-point Energies= -1489.697798 Hartree

Sum of electronic and thermal Energies= -1489.677505 Hartree

Sum of electronic and thermal Enthalpies= -1489.676561 Hartree

Sum of electronic and thermal Free Energies= -1489.750398 Hartree

Center Number	Coordinates (in Angstroms)			Center Number	Coordinates (in Angstroms)		
	X	Y	Z		X	Y	Z
1	-3.204579	0.465533	-0.171714	21	3.850782	0.143129	-1.515862
2	-1.971291	-0.189923	-0.504653	22	4.212114	0.953133	-0.514213
3	-0.869237	0.631664	-0.896923	23	3.215548	1.475791	0.209179
4	-0.962974	2.004527	-0.877607	24	1.856202	1.232398	0.006955
5	-2.159623	2.63318	-0.47678	25	-0.104959	2.625688	-1.126604
6	-3.266295	1.883019	-0.165131	26	-2.161649	3.719409	-0.397086
7	-4.345419	-0.306391	0.168586	27	-4.201393	2.362987	0.128047
8	-4.289741	-1.679929	0.208521	28	-5.272209	0.219177	0.405334
9	-3.070139	-2.335997	-0.058684	29	-5.172824	-2.265275	0.470246
10	-1.947493	-1.612472	-0.392388	30	-2.983043	-3.420418	0.010199
11	-0.803653	-2.357347	-0.635078	31	0.287399	4.058819	1.313114
12	0.251705	-0.015419	-1.377439	32	1.128258	1.754184	0.634673
13	0.232404	-2.251599	0.240368	33	3.501537	2.154507	1.015324
14	1.517398	0.386434	-1.047416	34	4.664697	-0.283434	-2.109847
15	1.406779	-2.92233	-0.101867	35	2.285059	-0.835601	-2.654308
16	2.48977	-2.835383	0.764099	36	3.425272	-3.341477	0.511208
17	2.486119	-2.150532	1.913007	37	1.466897	-3.475051	-1.038608
18	1.352168	-1.513293	2.214894	38	-0.683692	-0.969048	1.739
19	0.197067	-1.530714	1.434928	39	1.358124	-0.93491	3.141678
20	2.534021	-0.168765	-1.829108				

- [1] H. E. Gottlieb, V. Kotlyar, A. Nudelman, *J. Org. Chem.* **1997**, *62*, 7512–7515.
- [2] G. M. Sheldrick, *Acta Crystallogr. Sect. Found. Adv.* **2015**, *71*, 3–8.
- [3] G. M. Sheldrick, *Acta Crystallogr. Sect. C Struct. Chem.* **2015**, *71*, 3–8.
- [4] O. V. Dolomanov, L. J. Bourhis, R. J. Gildea, J. A. K. Howard, H. Puschmann, *J. Appl. Crystallogr.* **2009**, *42*, 339–341.
- [5] J. Contreras-García, E. R. Johnson, S. Keinan, R. Chaudret, J.-P. Piquemal, D. N. Beratan, W. Yang, *J. Chem. Theory Comput.* **2011**, *7*, 625–632.
- [6] H. S. Rzepa. <https://www.ch.ic.ac.uk/rzepa/cub2nci/>.
- [7] E. F. Pettersen, T. D. Goddard, C. C. Huang, G. S. Couch, D. M. Greenblatt, E. C. Meng, T. E. Ferrin, *J. Comput. Chem.* **2004**, *25*, 1605–1612.